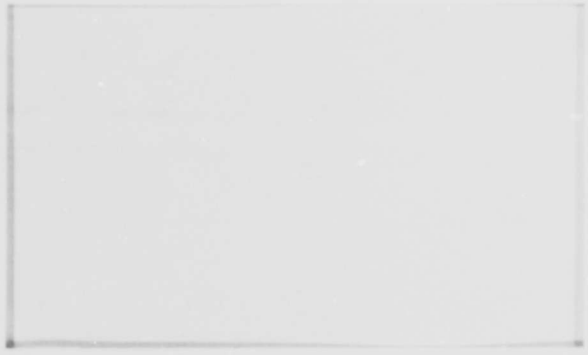

HYDRONAUTICS, incorporated
research in hydrodynamics

Research, consulting, and advanced engineering in the fields of NAVAL and INDUSTRIAL HYDRODYNAMICS. Offices and Laboratory in the Washington, D. C. area: Pindell School Road, Howard County, Laurel, Md.

UNCLASSIFIED

Security Classification

DOCUMENT CONTROL DATA - R & D

Security classification of title, body of abstract and indexing annotation must be entered when the overall report is classified)

1 ORIGINATING ACTIVITY (Corporate author) HYDRONAUTICS, Incorporated 7210 Pindell School Road, Howard County, Laurel, Maryland 20810	2a. REPORT SECURITY CLASSIFICATION Unclassified 2b. GROUP

3 REPORT TITLE

Scaling Laws for Cavitation Erosion

4 DESCRIPTIVE NOTES (Type of report and inclusive dates)

Technical Report

5 AUTHOR(S) (First name, middle initial, last name)

A. Thiruvengadam

6 REPORT DATE December 1971	7a. TOTAL NO. OF PAGES 70	7b. NO. OF REFS 52
8a. CONTRACT OR GRANT NO N00014-70-C-0204 NR 062-293 b. PROJECT NO. c. d.	9a. ORIGINATOR'S REPORT NUMBER(S) T. R. 233-15 9b. OTHER REPORT NO(S) (Any other numbers that may be assigned this report)	

10. DISTRIBUTION STATEMENT

Approved for public release; distribution unlimited.

11. SUPPLEMENTARY NOTES	12. SPONSORING MILITARY ACTIVITY Office of Naval Research Department of the Navy

13. ABSTRACT

In this report, six scaling laws are derived and used to investigate the feasibility of modeling cavitation erosion. The velocity scale and size scale are governed by the six nondimensional ratios, namely, the erosion number, the relative nuclei size, the Weber number, the cavitation number, the cavitation inception number and the degree of cavitation. These scaling laws indicate that it is possible to model erosion in the laboratory and to predict the prototype performance. In addition, these scaling laws explain many currently available experimental observations. For example, both Knapp's sixth power law for the dependence of erosion intensity on velocity, and the reported contradictions to this law, the influence of the cavitation number and the effect of model size can all be explained reasonably well with these new scaling laws. However, the complex nature of the phenomenon of cavitation erosion requires the adoption of several simplifying assumptions in the analysis. These assumptions and limitations are also discussed.

DD FORM 1 NOV 65 1473 (PAGE 1)

S/N 0102-014-6700

UNCLASSIFIED

Security Classification

D-23822

14 KEY WORDS	LINK A		LINK B		LINK C	
	ROLE	WT	ROLE	WT	ROLE	WT
Cavitation erosion						
Scaling laws						
Erosion number						
Nuclei size						
Weber number						
Liquid properties						
Cavitation number						
Time scale						
Velocity scale						
Size scale						
Modeling technique						
Knapp's Sixth power law						
Influence of cavitation number						
Material parameters						
Exposure time						

HYDRONAUTICS, Incorporated

TECHNICAL REPORT 233-15

SCALING LAWS FOR CAVITATION EROSION

By

A. Thiruvengadam

December 1971

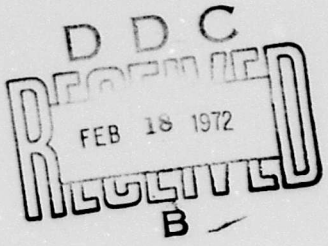

Prepared for

Office of Naval Research
Department of the Navy
under
Contract No. N00014-70-C-0204
NR 062-293

TABLE OF CONTENTS

LIST OF FIGURES

LIST OF TABLES

LIST OF NOTATIONS

C	speed of sound in the liquid
$C_{p_{min}}$	minimum pressure coefficient
d	diameter of the nuclei
$\bar{d}$	mean diameter
d^*	critical diameter of the nucleus
f	frequency of collapse
I_e	intensity of erosion
ℓ	characteristic length
m	meter
M	Mach number
n	cumulative number corresponding to the diameter d
n_o	cumulative number of nuclei that pass through a given point
n^*	cumulative number corresponding to the critical diameter
N	number of indentations in interval Δt

p_i	free stream pressure at inception of cavitation
p_{min}	the minimum pressure on the boundary
p_o	free stream pressure
p_v	vapor pressure
P_c	collapse pressure
P_i	impact pressure
P_o	initial pressure surrounding the bubble
Q_o	the partial pressure of the gas at the beginning of the collapse
R	bubble radius
R_c	final collapse radius
R_j	radius of the jet
R_o	initial radius of the bubble
S_e	erosion strength
V_o	free stream velocity
w	watts
W	Weber number

α	shape parameter in the Weibull distributions
γ	surface tension of the liquid at bubble wall
δ	relative nuclei size
Δt	exposure interval
Δy	mean depth of erosion
$\Delta y'$	depth of indentation due to a single impact
$\Delta\sigma$	degree of cavitation
Θ	erosion number
ρ	density of the liquid
σ	cavitation number
σ_i	cavitation number at inception
τ_g	bubble growth time

SUMMARY

Cavitation erosion is an important problem in many hydraulic and marine engineering systems. This report deals with some of the engineering aspects of this problem, especially from a designer's point of view. Preliminary design as well as redesign would be greatly aided by the development of model testing techniques. As of now there are no scaling laws governing this phenomenon. It is the objective of this report to develop such scaling laws and to investigate the feasibility of modeling cavitation erosion. The three important parameters to be scaled are the exposure time, speed and size.

It appears practical to conduct model tests over a shorter time by using a weaker material in the model. However, selection of model material depends upon several factors such as corrosion, structural strength, reproducibility of results and the techniques employed in the manufacture of models.

The velocity scale and size scale are governed by six nondimensional ratios, namely, the erosion number, the relative nuclei size, the Weber number, the cavitation number, the cavitation inception number and the degree of cavitation. These scaling laws indicate that it is possible to model erosion in the laboratory and to predict the prototype performance. In addition, these scaling laws explain many currentl available experimental observations. For example, both Knapp's sixth power law for the dependence of erosion intensity on velocity, and reported contradictions to this law, the influence of the cavitation number

and the effect of model size can all be explained reasonably well with these new scaling laws. However, it is recognized that cavitation erosion is a complex process; the analysis presented in this report has many limitations and simplifying assumptions. Further investigations are required to remove some of these limitations.

INTRODUCTION

Cavitation erosion is a serious problem in hydraulic turbines, pumps (1,2), valves, control devices, hydraulic structures, sluices, energy dissipators (3), ship propellers, hydrofoils (4), bearings (5), diesel engines (6), aircraft engines, torque converters, sonar domes, acoustic signal devices and processing and cleaning equipment, to mention only a few. Cavitation erosion is caused by the collapse of bubbles at or near solid boundaries which guide high speed flows. Good state-of-the-art reviews of the details of this phenomenon are available in References (7), (8) and (9).

With increasing requirements of higher speeds and smaller sizes for liquid-flow systems, the designer is confronted with cavitation erosion as an important limitation. Figure 1 shows the various engineering aspects of this problem from a designer's point of view. Basic research on bubble growth and collapse, material erosion and environmental interaction has generated much needed fundamental knowledge. The relative resistance of

many materials has also been catalogued using one of several screening tests. Tests commonly used include: (1) the vibratory tests, (2) the rotating disk test, (3) the Venturi test and (4) the jet impact test (8). Basic research combined with screening tests has led to several useful protection techniques which include the use of more resistant materials (inlays, overlays and elastomeric coatings), and the cathodic protection and air injection methods (10). These protection techniques are successful in some instances but not so useful in other cases.

Recent experiences with full scale systems show that in some cases even the most resistant material was severely eroded in short operational periods (4). If the erosion is serious at design conditions, the operational requirements such as capacity, power and speed might be relaxed. However, if the design is hopeless in terms of erosion intensity, then redesign is generally recommended. During redesign, one would correct obvious mistakes, avoid cavitation if at all possible and provide air vents at problem areas. It would be highly desirable to verify the redesign (or a preliminary design) with the help of a model test before costly manufacture is initiated. Such model tests would hopefully lead to the necessary modifications to a design so that the erosion intensity levels are within the capability of the candidate material. As of now there is no acceptable model testing technique, although some attempts have already been initiated in this direction (11,12,13). It is the purpose of this paper to consider the feasibility of developing such model tests and to examine the scaling laws governing the cavitation erosion phenomenon.

PRIMARY CONSIDERATIONS GOVERNING THE FEASIBILITY OF MODELING CAVITATION EROSION

The importance of developing model tests is obvious. However, the feasibility of such tests depends both upon economic aspects and technical considerations. For example, the cost of the test facility depends upon its size, which in turn governs the auxiliary machinery components such as pump and motor. Model size and test speed determine the capacity and cost of these components. Similarly operating costs are governed by testing time and model costs.

In technical terms, the feasibility of model testing depends upon the knowledge of the following three important scaling parameters in addition to several other considerations: (1) time scale, (2) velocity scale, and (3) size scale. The technical considerations dealing with these scales are discussed in the following sections.

Time Scale

Usually prototype systems are required to operate without erosion for a long time, typically greater than 10,000 hours. It becomes essential to develop scaling techniques with which one could shorten the test duration for the model test. It is now well established that the rate of erosion is a nonlinear function of the exposure period (8,10,14). The rate of erosion increases from negligible values, reaches a maximum, then decreases and

levels off to a steady value. A typical curve is shown in Figure 2. Such relations for a spectrum of materials are shown in Figure 3. The erosion time for these materials varies over a time scale from a few minutes to a few days.

Recently, Thiruvengadam (15) investigated the relationship between the relative rate of erosion (the ratio between the rate of erosion and the peak rate of erosion) and the relative exposure time (the ratio between the exposure time and the time corresponding to the peak erosion rate (Figure 4). A recently developed theory has also been correlated with these experimental data. This approach offers the possibility of using a weaker material to learn about the erosion potential of the prototype material at comparable intensities of erosion. The selection of materials for the model will be governed by several requirements such as structural strength, environmental effects, reproducibility of results and techniques employed in the manufacture of the models, in addition to the considerations involving test duration. The influence of corrosion on model-prototype correlation is currently unknown.

Velocity and Size Scales

The next important parameters are velocity and size scales. Knapp (16,17) conducted pioneering experiments to relate the rate of erosion with velocity and size. He measured the number of pits per unit area per unit time on an ogive body made of soft

annealed aluminum at various speeds in a water tunnel. Knapp found that the number of pits/sec/in^2 (which he called the intensity) varied as the sixth power of the velocity at a selected cavitation number (Figure 5). He compared these laboratory data with his measurements in a full scale hydraulic turbine operating in the field. His field measurements at one velocity were very close to the laboratory measurements at the same velocity (Figure 5), in spite of the different geometry and size of the field system. From these investigations, Knapp concluded that the intensity is solely a function of speed and does not depend upon the size or shape of the flow system.

However, experiments by Shalnev (18) and Thiruvengadam (19) showed that the rate of erosion varied significantly with the length of the cavity (cavitation cloud) at a given velocity. These observations raised serious doubts about Knapp's conclusions. In order to further understand these effects, additional experiments were conducted at the U. S. Naval Applied Science Laboratory using their rotating disk apparatus. Circular holes of 0.375 inch diameter were drilled at various locations on a circular disk made of 304 stainless steel and rotated for 48 hours at a chamber pressure of 15 psig (20). Further details of this apparatus may be found in Reference 21. The results are shown in Figure 6. Since the depth of erosion varied over the eroded area, the depth of erosion averaged over the eroded area is plotted against the peripheral speed in Figure 6. In contrast to Knapp's

sixth power law, the rate of erosion increased with velocity to a maximum and then decreased with increasing velocity. These apparently contradictory results which were the only data available during the early sixties, warranted a more detailed investigation of these effects.

The rotating foil apparatus fully described in earlier references (22,23) was specifically developed for these studies. Figure 7 shows an overall view of this facility. Systematic experiments were conducted on NACA 16-021 hydrofoils using this apparatus. Two sizes of the foil (3 inches and 1-1/2 inches in chord length) were tested. The rate of erosion was determined as a function of exposure time for each set of test conditions, lasting over cumulative exposure periods ranging from 10 hours to 70 hours depending upon the intensity of erosion. A typical plot of rate of erosion as a function of exposure period is shown in Figure 8. Both velocity and pressure were varied independently; these experimental results have been reported in References 22 and 13.

These investigations clearly established that the rate of erosion depended greatly on the exposure time, clarifying some of the controversies on this aspect of the phenomenon (24). There was an incubation period during which there was no measurable weight loss. Following the incubation period, there was a period of accelerating erosion rates. After reaching a maximum

value, the rate of erosion decreased with a tendency toward a steady state. The maximum rate of erosion was highly dependent on the cavitation number at a given velocity. The erosion rate increased with decreasing cavitation number, reached a maximum value and then decreased with further reduction in the value of cavitation number as shown in Figure 9. The intensity of erosion represented by the ordinate of this figure is given by

$$I_e = \frac{\Delta y}{\Delta t} S_e \qquad [1]$$

where Δy is the average depth of erosion over the eroded area in a given exposure interval of Δt, and S_e is the erosion strength (26).

The results shown in Figure 9 demonstrate that the intensity of cavitation erosion depends upon the velocity and the size of the foil in addition to the cavitation number. For example, the three inch foil at 175 fps has a peak intensity of 1.2 w/m^2 which occurs at a cavitation number of 0.30; whereas for the 1-1/2 inch foil at the same velocity the peak intensity is only 0.6 w/m^2 at a cavitation number of 0.36. The maximum rates corresponding to the optimum cavitation numbers are plotted against velocity in Figure 10. The solid line in this figure corresponds to Knapp's sixth power law. An understanding of the velocity scale effect and the size scale effect observed in these experiments is crucial to the eventual development of modeling techniques for predicting cavitation erosion. The following analysis was motivated by this objective.

SCALING LAWS FOR CAVITATION EROSION

Spherical Collapse

It is now generally accepted that high pressures caused by the collapse of bubbles produce deformation and material failure. As early as 1917, Rayleigh (27) attempted to show that such high pressures are possible during bubble collapse. Rayleigh's analysis of an empty bubble collapsing in an incompressible liquid predicted infinite bubble wall velocities and collapse pressures (Figure 11). He obviated this difficulty by introducing a perfect gas obeying Boyle's law in the bubble. Furthermore, he knew that a satisfactory theory should take into account the compressibility of the liquid. Realizing the importance of compressibility effects in bubble collapse, several investigators including Hickling and Plesset (28) and Ivany and Hammit (29) considered this effect in their calculations. While surface tension tends to increase the rate of collapse, compressibility, viscosity and noncondensible gas in the bubble tend to slow down the collapse rate (30). The influence of viscosity on collapse rate is negligible except for large bubbles.

Nonspherical Collapse

Recent attention has been directed toward an understanding of nonspherical collapse. However, interest in the formation of liquid jets arising out of nonspherical collapse may be traced to early investigators. For example, Eisenberg (31),

as early as 1950, hypothesized the formation of liquid jets caused by the "unsymmetrical collapse of cavitation bubbles in a pressure gradient." Suvorov (32) and Naude and Ellis (33) observed experimentally the formation of such jets during the later stages of bubble collapse. Naude and Ellis (33) photographed such jets and the indentations caused by these jets. Hancox and Brunton (34) and Thiruvengadam et al (35) have shown that multiple impacts by water jets can cause erosion even at impact speeds in the range of 100 fps. More recently, Benjamin and Ellis (36), Tulin (37), Mitchell and Hammitt (38) and Plesset and Chapman (39) have all contributed to the understanding of the jet impact mechanism. It is interesting to note that the theoretical prediction of the micro-jet formation in front of the primary jet (Figure 12) is very similar to the experimental "Monroe Jet" observations of Bowden and Brunton (40).

Indentation and Rate of Erosion

If the stress caused by the collapse of the bubble exceeds the yield strength of the material, a permanent dent may be produced by a single impact. However, even if the collapse stress is less than the yield strength, a dent may still be produced after several collapses due to fatigue failure of the material. The actual fracture of a particle from the surface of the material may be produced from overlapping indentations caused by the collapse of many bubbles. For a single impact, the depth of indentation, $\Delta y'$, may be approximately related to the strength

of the material, S_e, the impact pressure, P_i and the size of the shock or jet, R, by the following relationship*

$$\Delta y' \cdot S_e \propto P_i \cdot R \qquad [2]$$

If we use the simple analogy of a hardness test (41, 42, 43), the strength, S_e, corresponds to the appropriate hardness of the material. For the case of multiple impacts with a frequency of f, the rate of indentation may be approximated by

$$\frac{\Delta y}{\Delta t} \cdot S_e \propto P_i \cdot R \cdot f \qquad [3]$$

The left side of relation [3] represents the intensity of erosion, as given by relation [1], whereas the right side is the intensity of bubble collapse. These ideas were initiated as early as 1960 (44, 45). The details of the derivations for relations [2] and [3], including assumptions and limitations, are contained in the appendix.

---

* The sign $\propto$ means "is proportional to". All the constants of proportionality are omitted in the derivations since we are interested only in nondimensional ratios.

For a sufficiently shallow indentation of predominantly plastic character, the diameter of indentation, d is proportional to $\sqrt{R \cdot \Delta y'}$. This result, when used with conventional relationships for hardness, will lead to relation [2]. Ideal plasticity is assumed. If the impact stress is much larger than the yield strength of the material, deep craters and associated plastic flow are produced on the surface of the material. This analysis is mainly applicable to materials that are neither too soft nor too strong, i.e., with yield strengths of the same order of magnitude as the impact stress.

The intensity of bubble collapse depends upon three parameters, namely the impact pressure, P_1, the size of the bubble or jet and the frequency of impact. The approach in this report is to relate these three parameters to hydrodynamic characteristics such as velocity, pressure and size of the system. As shown in Figure 13, we can classify the bubble collapse mechanisms into three categories, spherical collapse, macrojet impact and microjet impact. Rayleigh (27) and several other investigators considered the spherical collapse in detail. Plesset and Chapman (39) among others have considered the macrojet and microjet.

Spherical Collapse

The collapse pressure due to spherical collapse, P_c, is given by

$$P_c \propto P_o \left(\frac{R_o}{R_c}\right)^3 \qquad [4]$$

where P_o and R_o correspond to initial pressure and radius and R_c is the final collapse radius. If the center of collapse is of the order of the initial radius, the impact pressure, P_1, is given by

$$P_1 \propto P_o \left(\frac{R_o}{R_c}\right)^3 \qquad [5]$$

allowing for a (1/radius) attenuation (46). The relative radius, R_o/R_c, depends upon many factors including surface tension,

noncondensible gas, heat transfer effects and compressibility of the liquid (30). For example, the influence of noncondensible gas obeying Boyle's law was given by Rayleigh (27) as

$$\frac{R_o}{R_c} \propto \exp\left(\frac{P_o}{Q_o}\right)^{\frac{1}{3}} \qquad [6]$$

where Q_o is the partial pressure of the gas at the beginning of the collapse. Similarly, other effects may also be evaluated (11).

Jet Impact

The pressure caused by the jet may be classified into two categories: (1) the stagnation pressure developed by a long jet acting for a large duration, and (2) the water hammer pressure resulting from a short jet of small duration. According to Plesset and Chapman (39), velocity of the jet is proportional to $\sqrt{P_o}$. Then the stagnation pressure is proportional to P_o, whereas the water hammer pressure is proportional to $C\sqrt{\rho P_o}$; C is the sound speed and ρ is the density of the liquid;

$$P_i \propto P_o \quad \text{(for the case of stagnation pressure)} \qquad [7]$$

$$P_i \propto C\sqrt{\rho P_o} \quad \text{(for the case of water hammer pressure)} \qquad [8]$$

Growth of Bubbles

The initial size of the bubble at the beginning of the collapse is related to the time available for growth and the pressure difference between the inside and the outside of the bubble (47), Figure 14. The growth time, τ_g, is directly proportional to the length of travel of the bubble and inversely proportional to the translational velocity of the bubble. The travel length is proportional to the cavity length which is proportional to the model length at a given cavitation number. Experimental observations by Ivany, Hammitt and Mitchel (48) show that the bubbles move at approximately the same speed as the liquid. The pressure causing growth is related to the difference between the vapor pressure, p_v, and the minimum pressure, p_{min}. The surface tension is neglected, but it is possible to account for it. These relationships may be written as follows:

$$R_o \propto \tau_g \sqrt{\frac{\Delta p}{\rho}} \qquad [9]$$

$$\tau_g \propto \frac{l}{V_o} \qquad [10]$$

$$\Delta p \propto p_v - p_{min} \qquad [11]$$

Combining these equations and using the well known relations for the cavitation number, σ, and the minimum pressure coefficient, $C_{p_{min}}$, given by

$$\sigma = \frac{p_o - p_v}{\frac{1}{2}\rho V_o^2} \qquad [12]$$

and

$$C_{p_{min}} = \frac{p_{min} - p_o}{\frac{1}{2}\rho V_o^2} \qquad [13]$$

and assuming that σ_i, the cavitation inception number is

$$\sigma_i = - C_{p_{min}} \quad \text{(See Johnson (49))} \qquad [14]$$

we get

$$R_o \propto \ell \, (\sigma_i - \sigma)^{\frac{1}{2}} \qquad [15]$$

Moreover, the radius of the jet, R_j, is assumed as:

$$R_j \propto R_o \qquad [16]$$

Frequency of Bubble Growth and Collapse

As discussed earlier, the rate of erosion is related to the number of bubbles collapsing per unit time at a given location. The number of bubbles that collapse is related to the number of bubbles that become unstable and grow. Some of the parameters that affect the bubble instability are:

1. Nuclei size,
2. Surface tension,
3. Velocity,
4. Pressure, and
5. Size of the model.

Recently Johnson (49) considered these parameters and demonstrated that bubbles smaller than tne critical size do not grow under a given set of flow conditions (Figure 15). For example, bubbles of the order of 10^{-4} in. in diameter may not grow at speeds less than 60 fps whereas they may become critical at a speed of 120 fps, as shown in Figure 15.

In n_o is the cumulative number of nuclei that pass a given point in a given time interval, then one can plot a distribution of sizes of these bubbles as shown in Figure 16. The relative nuclei size is $d/\bar{d}$ where $\bar{d}$ is tne mean diameter and n is the cumulative number corresponding to the diameter d. As of now, there are no systematic measurements of such distributions in practical flow systems. However, if we assume that the nuclei size is governed by a Weibull type of distribution, then

$$\frac{n}{n_o} = \exp\left[-\left(\frac{d}{\bar{d}}\right)^{\alpha}\right] \qquad [17]$$

where α is the Weibull shape parameter. It is easily recognized that the Weibull distribution gives the simple exponential distribution when $\alpha = 1$, the Rayleigh distribution when $\alpha = 2$, and approximates the normal distribution when $\alpha = 3.57$ (50).

According to Johnson (49),

$$d^* = \frac{8\gamma}{3(p_v - p_{min})} \qquad [18]$$

where

d^* = the critical diameter of the nucleus, and

γ = the surface tension of the liquid.

Then

$$\frac{d^*}{\bar{d}} = \frac{8}{3} \frac{\gamma}{(\sigma_1 - \sigma)\ \frac{1}{2}\rho V_o^2\ \bar{d}} \qquad [19]$$

$$= \frac{2.67}{W\ (\sigma_1 - \sigma)} \qquad [20]$$

where $W = \dfrac{\frac{1}{2}\rho V_o^2\ \bar{d}}{\gamma}$ is the Weber number.

If n^* corresponds to d^*, then a simple exponential distribution for the nuclei size would yield:

$$\frac{n^*}{n_o} = \exp\left[-\frac{d^*}{\bar{d}}\right] \qquad [21]$$

$$= \exp\left[\frac{-2.67}{W(\sigma_1 - \sigma)}\right] \qquad [22]$$

Physically, one can infer that n_o is related to the flow speed and the mean size of the nuclei. Hence,

$$n_o \propto \frac{V_o}{\bar{d}} \qquad [23]$$

$$n^* \propto \frac{V_o}{\bar{d}} \exp -\left[\frac{2.67}{W(\sigma_i - \sigma)}\right] \qquad [24]$$

Scaling Laws for Cavitation Erosion

So far, we have discussed the relationships governing the impact pressure, the size of the bubble or the jet, and the number of bubbles collapsing per unit time. We also showed in this section that the intensity of bubble collapse is the product of these parameters. For example, the jet impact case reduces to

$$I_e \propto P_i \cdot R_j \cdot f \quad ; \quad P_i \propto p_o$$

$$\propto p_o \ell (\sigma_i - \sigma)^{\frac{1}{2}} \frac{V_o}{\bar{d}} \exp\left[\frac{-2.67}{W(\sigma_i - \sigma)}\right] \qquad [25]$$

Relation [25] is obtained by combining [1], [3], [7], [14] and [24]. Again,

$$p_o - p_v = \sigma \tfrac{1}{2}\rho V_o^2$$

But

$$p_v \ll p_o \text{ for practical cases of erosion.}$$

Then

$$p_o \approx \sigma \tfrac{1}{2}\rho V_o^2$$

Hence

$$I_e \propto \tfrac{1}{2}\rho V_o^3 \frac{\ell}{\bar{d}} \sigma(\sigma_i - \sigma)^{\frac{1}{2}} \exp\left[\frac{-2.67}{W(\sigma_i - \sigma)}\right] \qquad [26]$$

Rearranging [26] in non-dimensional groups, we obtain,

$$\Theta = \frac{\sigma}{\delta} (\Delta\sigma)^{\frac{1}{2}} \exp\left[-\frac{2.67}{W(\Delta\sigma)}\right] \qquad [27]$$

as an expression for the erosion number, Θ, for the jet impact case; where

$$\Theta = \frac{I_e}{\tfrac{1}{2}\rho V_o^3} \quad - \text{ Erosion number} \qquad [28]$$

$$\delta = \frac{\bar{d}}{\ell} \quad - \text{ Relative nuclei size} \qquad [29]$$

$$W = \frac{\tfrac{1}{2}\rho V_o^2 \bar{d}}{\gamma} \quad - \text{ Weber number} \qquad [30]$$

$$\sigma = \frac{p_o - p_v}{\tfrac{1}{2}\rho V_o^2} \quad - \text{ Cavitation number} \qquad [31]$$

$$\sigma_i = \frac{p_i - p_v}{\tfrac{1}{2}\rho V_o^2} \quad - \text{ Cavitation inception number} \qquad [32]$$

$$\Delta\sigma = (\sigma_i - \sigma) \quad - \text{ Degree of cavitation} \qquad [33]$$

Similar results for the water hammer pressure produced by microjets and for spherical shocks produced by spherical collapse are summarized in Table 1.

If we examine the case of water hammer pressure, then

$$\Theta = \frac{\sigma}{\delta M} (\Delta\sigma)^{\frac{1}{2}} \exp\left[\frac{-2.67}{W(\Delta\sigma)}\right] \qquad [34]$$

where

$M = V_o/C$ = Mach number,

and

C = the speed of sound in the liquid.

For the case of spherical shock, we get

$$\Theta = \frac{\sigma}{\delta} (\Delta\sigma)^{\frac{1}{2}} \exp\left[\frac{2}{3}\left(\frac{p_o}{Q_o}\right) - \frac{2.67}{W(\Delta\sigma)}\right] \qquad [35]$$

where Q_o is the partial pressure of noncondensible gas in the bubble at the start of collapse.

Surface tension, compressibility and thermal effects may also be included for the case of spherical collapse. A discussion of these effects is available in Reference 11.

In essence, this section of the report leads to some of the important scaling laws governing the phenomenon of cavitation erosion. It is necessary to verify these scaling parameters with carefully planned experiments. In the meantime, an attempt was made in the next section to see if these scaling laws would explain the available experimental results.

ANALYSIS AND DISCUSSION OF RESULTS

According to Figure 9, the intensity of erosion increases with increasing cavitation number, reaches a maximum and then decreases to a negligible value at the cavitation inception number. Such a behavior is compatible with relations [27], [34], and [35]. Figure 17 shows a plot of the value of $\mathcal{E} \cdot \delta$ (Product of the erosion number and the relative nuclei size) as a function of cavitation number for various values of the cavitation inception number. These values are computed from the relationship [27] for a particular value of the Weber number. It is easily recognized that the experimental results in Figure 9 are in conformity with the theoretical results in Figure 17 qualitatively. According to Figure 17, the intensity would increase, reach a maximum and then decrease when cavitation parameter is varied, keeping all the other non-dimensional ratios constant.

The experimental results in Figure 9 further show that the size of the hydrofoil has an influence on the intensity of erosion as well as on the cavitation number at which the maximun intensity occurs. This behavior is also compatible with relations [27], [34] and [35]. Changing the size of the foil changes both the relative nuclei size, δ, and the cavitation inception number, σ_i, thereby affecting the degree of cavitation, $\Delta\sigma$. The experimental results show that the maximum intensity for the 3-in. chord hydrofoil at 175 fps is about one half of that of 1-1/2 in. chord hydrofoil at the same speed.

The next important parameter is the velocity. Our experiments as well as earlier experiments of other investigators show that the intensity of erosion is proportional to $(V_o)^e$; the value of the exponent, e, has been reported to vary anywhere from 3 to 10 (18, 19, 51). This variation in the velocity exponent can also be explained by plotting $\Theta\delta/\sigma(\Delta\sigma)^{\frac{1}{2}}$ as a function of Weber number for various values of $\Delta\sigma$, from Equation [27] as shown in Figure 18. For nuclei sizes on the order of 10^{-5} ft in water, for a speed range of 100 to 200 fps, the Weber number would be on the order of 20 to 80. For most of the experiments the degree of cavitation ($\Delta\sigma$) was close to optimum (around 0.1). Keeping δ, σ, and $\Delta\sigma$ constant, we see in the shaded region in Figure 18, that the following approximate relation exists:

$$\Theta \propto W^{1.5} \qquad [36]$$

From Equation [30],

$$W \propto V_o^2 \qquad [37]$$

and from Equation [28]

$$I_e \propto \Theta V_o^3 \qquad [38]$$

Combining Equations [36], [37] and [38], we find that

$$I_e \propto V_o^6 \qquad [39]$$

which is a justification for Knapp's sixth power law for the dependence of erosion on velocity. Similarly, the other values of velocity exponents can be explained depending upon the values of

W and $\Delta\sigma$ for each specific experiment. Table 2 shows the range of nuclei size, velocities and Weber numbers that are of interest in model-prototype correlations. As shown in Figure 18, the erosion number, θ, becomes independent of Weber number for $W > 1000$ and $\Delta\sigma \sim 0.1$. The nuclei size and surface tension have to be controlled in order to keep δ constant and at the same time to maintain $W > 1000$.

The discussions above have attempted to probe into some of the important experimental results in terms of the scaling parameters suggested in this report. The roles played by cavitation number, velocity and size of the system are compatible with the analysis. The phenomenon of cavitation erosion is a very complex process. The discussions and analyses presented in this report are only a first step, with much more remaining to be understood. There are several limitations to these analyses which are enumerated in the next section.

LIMITATIONS AND ASSUMPTIONS

(1) The complexity of the phenomenon of cavitation erosion necessitates several simplifying assumptions that have been implicitly and explicitly made in this paper. Although these assumptions seem to be physically realistic, further investigations are required to verify them.

(2) The influence of corrosion on the long term erosion behavior of candidate materials at relatively lower erosion intensities is not well understood. This is a serious limitation in time scaling.

(3) The phenomenon of bubble collapse is statistical in nature. Similarly, the fracture of solid particles from the surface of the material is also a statistical process. Assigning a strength value or an energy value to the resistance of the material in this context is controversial, to say the least. The author's approach, represented by relation [3] is one of many different approaches, concepts and ideas that are forthcoming from several contemporary investigators.

(4) The primary objective of our current effort is the derivation of nondimensional parameters that may serve as scaling laws. Within the range of experimental data currently available for analysis, these scaling laws have been shown to be meaningful. However, it remains to be seen how far these laws may be extended.

(5) The role of noncondensible gas, compressibility, surface tension, viscosity and heat transfer effects in the nonspherical collapse are currently being investigated. Plesset and Chapman (39) have discussed the relative influence of these parameters.

(6) As discussed earlier, the inception of cavitation depends both on free nuclei as well as on surface nuclei (52). Only the case of free nuclei has been considered in this report. However, it is possible to extend the same approach to the surface nuclei case. It is also necessary to investigate different nuclei distribution functions. For example Figure 19 shows the influence of the Weibull shape parameter for a given degree of cavitation; the shape parameter has no appreciable influence for Weber numbers greater than 30, which is the practical range.

(7) Similar to the statistical distribution for bubble growth, there is likely to be another distribution for the number of bubbles collapsing near the material surface. Future investigations may also have to take this aspect into consideration.

(8) Presently available experimental results on the effects of cavitation parameter, velocity and size of the model are compatible with the approximate analysis using the stagnation pressure caused by the dynamic action of the jet. Additional investigations are needed to explore the implications of the water hammer pressure and shock wave cases.

(9) It is recognized that what is presented in this paper is only a step toward an important goal of developing techniques for modeling cavitation erosion to help designers and engineers.

CONCLUDING REMARKS

The importance of model tests to determine the intensity of erosion of full scale systems is obvious. Time scale, velocity scale and size scale are the three important scales in modeling cavitation erosion. The technical feasibility of scaling these parameters is discussed in this report.

A weaker (less resistant to erosion) material may be used to learn about the erosion potential of the prototype. This approach offers the possibility of shortening the time required to test models in the laboratory. However, the selection of modeling materials will be governed by several factors including corrosion, structural strength, reproducibility of results and model making techniques. The influence of corrosion on model-prototype correlation is currently unknown.

The analysis presented shows that the intensity of cavitation erosion experienced in a flow system is related to the following six scaling parameters:

1. $\theta = \dfrac{\frac{\Delta V}{\Delta t} \cdot S_e}{\frac{1}{2}\rho V_o^3}$ - Erosion number

2. $\delta = \dfrac{\bar{d}}{\ell}$ - Relative nuclei size

3. $W = \frac{\frac{1}{2}\rho V_o^2 \bar{d}}{\gamma}$ - Weber number

4. $\sigma = \frac{p_o - p_v}{\frac{1}{2}\rho V_o^2}$ - Cavitation number

5. $\sigma_i = \frac{p_i - p_v}{\frac{1}{2}\rho V_o^2}$ - Cavitation inception number

6. $\Delta\sigma = (\sigma_i - \sigma)$ - Degree of cavitation

The erosion number represents the efficiency of erosion. It depends upon the cavitation number, the degree of cavitation and the relative nuclei size at a given Weber number. For given values of the relative nuclei size, the cavitation number and the degree of cavitation, the erosion number varies as an exponential function of the Weber number. At large values of the Weber number, the erosion number becomes independent of the Weber number. These results are compatible with available experimental observations. For example, Knapp's sixth power law, observed contradictions to this law, effect of cavitation number and effect of size of the model can all be explained reasonably well with the present analysis.

These investigations lead to some guidelines in the selection of the velocity scale, model size scale, the nuclei size scale, the surface tension of the test liquid and the degree of cavitation during the planning stage of a model test program. As pointed out earlier, there are several limitations to this approach. Further carefully planned experimental research is required before any final recommendation can be made. It is fair to conclude that the feasibility of conducting reliable model tests seems very promising.

APPENDIX

1. Indentation and Rate of Erosion

$$\text{Force} \propto R^2 P_i \quad \text{(force causing indentation)} \qquad [A1]$$

$$\text{Resisting force} \propto d^2 S_e \quad \text{(For perfectly plastic case)} \qquad [A2]$$

where d is the diameter of indentation (See Figure 13). For small indentations, equating [A1] and [A2]

$$d^2 \propto \Delta y' \cdot R \qquad [A3]$$

Hence, (see Figure 13)

$$\Delta y' \cdot S_e \propto P_i R \qquad [A4]$$

For multiple indentations at a frequency of f, there will be $N = f \cdot \Delta t$ indentations in an interval, Δt. Then,

$$N \cdot \Delta y' \cdot S_e \propto P_i \cdot R \cdot f \cdot \Delta t \qquad [A5]$$

$$\frac{N \Delta y'}{\Delta t} \cdot S_e \propto P_i R \cdot f \qquad [A6]$$

Let $\Delta y = N \Delta y'$, the depth eroded in Δt.

Then,

$$\frac{\Delta y}{\Delta t} \cdot S_e \propto P_i \cdot R \cdot f \qquad [A7]$$

2. **Bubble Size**

$$R_o \propto \tau_g \sqrt{\frac{\Delta p}{\rho}} \qquad [A8]$$

$$\tau_g \propto \frac{\ell}{V_o} \qquad [A9]$$

$$\Delta p \propto p_v - p_{min} \qquad [A10]$$

$$R_o \propto \frac{\ell}{V_o} \sqrt{\frac{p_v - p_{min}}{\rho}} \qquad [A11]$$

$$\propto \ell \sqrt{\frac{p_v - p_o + p_o - p_{min}}{\frac{1}{2}\rho V_o^2}} \qquad [A12]$$

$$\propto \ell \sqrt{(-C_{p_{min}} - \sigma)} \qquad [A13]$$

If we assume $C_{p_{min}} = -\sigma_i$ (Johnson (49))

Then

$$R_o \propto \ell \, (\sigma_i - \sigma)^{\frac{1}{2}} \qquad [A14]$$

3. **Jet Size**

$$P_o R_o^3 \propto \rho R_j^2 L_j \cdot V_j^2 \qquad [A15]$$

where

R_j = Radius of the jet,
L_j = Length of the jet, and
V_j = Velocity of the jet.

If

$$\tfrac{1}{2}\rho V_j^2 \propto P_o \qquad [A16]$$

and

$$L_j \propto R_j \qquad [A17]$$

Then,

$$R_j \propto R_o \qquad [A18]$$

4. Number of Bubbles Growing and Collapsing

$$d^* = \frac{8\gamma}{3(p_v - p_{min})} \qquad \text{Johnson (49)} \qquad [A19]$$

$$\frac{d^*}{\bar{d}} = \frac{2.67\ \gamma}{(\sigma_1 - \sigma)\ \tfrac{1}{2}\rho V_o^2\ \bar{d}} \qquad [A20]$$

If n* corresponds to d*, then

$$\frac{n^*}{n} = \exp\left[-\frac{d^*}{\bar{d}}\right] \qquad [A21]$$

$$n^* = n_o \exp\left[-\frac{2.67}{W(\sigma_1 - \sigma)}\right] \qquad [A22]$$

If $n^* \propto f$ and $n_o \propto V_o/\bar{d}$, then

$$f \propto \frac{V_o}{\bar{d}} \exp\left[-\frac{2.67}{W(\sigma_1 - \sigma)}\right] \qquad [A23]$$

Rayleigh distribution for the nuclei

$$f \propto \frac{V_o}{\bar{d}} \exp\left[-\left\{\frac{2.67}{W(\sigma_1 - \sigma)}\right\}^2\right] \qquad [A24]$$

Approximate normal distribution for the nuclei

$$f \propto \frac{V_o}{\bar{d}} \exp\left[-\left\{\frac{2.67}{W(\sigma_1 - \sigma)}\right\}^{3.57}\right] \qquad [A25]$$

5. **Intensity of Collapse if we use Water Hammer Pressure of the Jet**

$$I_e \propto P_1 \cdot R \cdot f \; ; \quad P_o \propto p_o$$

$$\propto C\sqrt{\rho p_o} \cdot \ell \cdot (\sigma_1 - \sigma)^{\frac{1}{2}} \frac{V_o}{\bar{d}} \exp\left[-\frac{2.67}{W(\sigma_1 - \sigma)}\right] \qquad [A26]$$

$$p_o \propto \sigma \cdot \tfrac{1}{2}\rho V_o^2 \; ; \quad p_v \ll p_o$$

Then

$$I_e \propto \tfrac{1}{2}C \cdot \rho V_o^2 \frac{\ell}{\bar{d}} \sigma (\sigma_1 - \sigma)^{\frac{1}{2}} \exp\left[-\frac{2.67}{W(\sigma_1 - \sigma)}\right] \qquad [A27]$$

$$\propto \tfrac{1}{2}\rho V_o^3 \cdot \frac{C}{V_o} \cdot \frac{\ell}{\bar{d}} \sigma(\sigma_1 - \sigma)^{\frac{1}{2}} \exp\left[-\frac{2.67}{W(\sigma_1 - \sigma)}\right] \qquad [A28]$$

6. Intensity of Collapse if we use the Shock Wave Pressure

$$I_e \propto p_o \left(\frac{R_o}{R_c}\right)^3 \cdot \ell\,(\sigma_1 - \sigma)^{\frac{1}{2}} \frac{V_o}{d} \exp\left[-\frac{2.67}{W(\sigma_1 - \sigma)}\right] \qquad [A29]$$

$$\left(\frac{R_o}{R_c}\right)^3 = \exp\left(\frac{p_o}{Q_o}\right) \qquad [A30]$$

$$I_e \propto p_o \exp\left(\frac{2}{3}\frac{p_o}{Q_o}\right) \cdot \ell\,(\sigma_1 - \sigma)^{\frac{1}{2}} \frac{V_o}{d} \exp\left[-\frac{2.67}{W(\sigma_1 - \sigma)}\right] \qquad [A31]$$

$$\propto \tfrac{1}{2}\rho V_o^3 \frac{\ell}{d} \cdot \sigma\,(\sigma_1 - \sigma)^{\frac{1}{2}} \exp\left[\left(\frac{2}{3}\frac{p_o}{Q_o}\right) - \frac{2.67}{W(\sigma_1 - \sigma)}\right] \qquad [A32]$$

REFERENCES

1. Wood, G. M. and Whippen, W. G., "Cavitation Effects in Turbomachinery," ASME Symp. on Cavitation State of Knowledge, pp. 148-165, 1969.

2. Smith, P. G., DeVan, J. H., Grindell, A. G., "Cavitation Damage to Centrifugal Pump Impellers During Operation with Liquid Metals and Molten Salt at 1050-1400°F," Trans. ASME, Vol. 85, Series D., Jour. Basic Engineering, pp. 329-337, 1963.

3. Cavitation in Hydraulic Structures: A Symposium, Proc. Am. Soc. Civil Engrs., Vol. 71, No. 7, Sept. 1945.

4. Morgan, Wm. B., and Lichtman, J. Z., "Cavitation Effects on Marine Devices," ASME Symp. on Cavitation State of Knowledge, pp. 195-241, 1969.

5. Leith, W. C. and Thompson, A. L., "Some Corrosion Effects in Accelerated Cavitation Damage," Trans. ASME, Vol. 82, Series D, Jour. Basic Engineering, pp. 795-807, 1960.

6. Speller, F. N., and LaQue, F. L., "Water Side Deterioration of Diesel Engine Cylinder Liners," Corrosion, 6, No. 7, 1950, pp. 209-215.

7. Robertson, J. M., and Wislicenus, G. F. (Eds.), "Cavitation State of Knowledge," Symposium Proceedings, The American Society of Mechanical Engineers, 1969.

8. Eisenberg, P., "Cavitation and Impact Erosion - Concepts, Correlations, Controversies," ASTM STP 474, pp. 3-28, 1970.

9. Thiruvengadam, A., "Cavitation Erosion," Applied Mechanics Reviews, Vol. 24, No. 3, March 1971, pp. 245-253.

10. Eisenberg, P., Preiser, H. S., and Thiruvengadam, A., "On the Mechanisms of Cavitation Damage and Methods of Protection," Trans. Soc. Naval Arch. and Marine Engineers, Vol. 73, 1965, pp. 241-286.

11. Thiruvengadam, A., "On Modeling Cavitation Damage," Jour. Ship Research, Vol. 13, No. 3, pp. 220-233, September 1969.

12. Van der Meulen, J. H. J., "Cavitation Erosion of a Ship Model Propeller," Am. Soc. for Testing and Materials (ASTM) Spec. Tech. Publication 474, pp. 162-180, 1970.

13. Thiruvengadam, A., "Effect of Hydrodynamic Parameters on Cavitation Erosion Intensity," HYDRONAUTICS, Incorporated Technical Report 233-14, 1970.

14. Heymann, F. J., "On the Time Dependence of the Rate of Erosion Due to Impingement or Cavitation," ASTM STP 408, pp. 70-110, 1967.

15. Thiruvengadam, A., "On the Selection of Modeling Materials to Scale Long Term Erosion Behavior of Prototype Systems," Proc. of the Third International Conference on Rain Erosion and Allied Phenomena, Royal Aircraft Est. Farnborough, England, 1970.

16. Knapp, R. T., "Recent Investigations of the Mechanics of Cavitation and Cavitation Damage," Trans ASME Vol. 77, 1955, pp. 1045-1054.

17. Knapp, R. T., "Accelerated Field Test of Cavitation Intensity," Trans. ASME, Vol. 80, No. 1, pp. 91-102, 1958.

18. Shalnev, K. K., "Experimental Study of the Intensity of Erosion due to Cavitation," Proc. Symp. on Cavitation in Hydrodynamics, (N.P.L. 1955), H.M.S.O. 1956.

19. Thiruvengadam, A., "Cavitation and Cavitation Damage," M.Sc. Thesis, Dept. of Power Engineering, Indian Institute of Science, Bangalore-12, India, 1959.

20. Thiruvengadam, A., unpublished results, Materials Laboratory, New Yrok Naval Shipyard, 1963.

21. Kallas, D. H., and Lichtman, J. Z., "Cavitation Erosion," Environmental Effects on Polymeric Materials, Vol. 1, Chapter 2, Interscience, New York, 1968.

22. Kohl, R. E., "Experimental Studies to Establish Scaling Laws for Modeling Cavitation Damage," HYDRONAUTICS, Incorporated Technical Report 233-12, June 1968.

23. Thiruvengadam, A., and Conn, A. F., "Some Recent Techniques to Study the Behavior of Ocean Engineering Materials, Materials Research and Standards, An ASTM Journal, in press.

24. Eisenberg, P., Discussion of the paper by Plesset, M. S., and Devine, R. E., See Reference 25.

25. Plesset, M. S., and Devine, R. E., "Effect of Exposure Time on Cavitation Damage," Trans. ASME, Jour. Basic Eng., Vol. 88, No. 4, Series D, December 1966, pp. 691-705.

26. Thiruvengadam, A., "The Concept of Erosion Strength," ASTM STP 408, pp. 22-36, 1967.

27. Rayleigh, Lord, "On the Pressure Developed in a Liquid During the Collapse of a Spherical Cavity," Phil. Mag., Vol. 34, Series 4, 1917, pp. 94-98.

28. Hickling, R. and Plesset, M. S., "Collapse and Rebound of a Spherical Bubble in Water," Physics of Fluids, Vol. 7, pp. 7-14, 1964.

29. Ivany, R. D., and Hammitt, F. G., "Cavitation Bubble Collapse in Viscous Compressible Liquids - Numerical Analysis," Trans. ASME, 87, Series D., Jour. Basic Engrg., pp. 977-985, 1965.

30. Knapp, R. T., Daily, J. W., and Hammitt, I. G., Cavitation, McGraw-Hill, 1970.

31. Eisenberg, P., "On the Mechanism and Prevention of Cavitation," David Taylor Model Basin Report 712, Washington, D. C., 1950. (Earlier work by Ackeret and Mueller are referred to in this publication.)

32. Kornfeld, M., and Suvorov, L., "On the Destructive Action of Cavitation," Jour. Appl. Physics, Vol. 15, pp. 495-506, 1944.

33. Naude, C. F., and Ellis, A. T., "On the Mechanism of Cavitation Damage by Non-Hemispherical Cavities Collapsing in Contact with a Solid Boundary," Trans. ASME, Jour. Basic Engrg., Series D., Vol. 83, pp. 648-656, 1961.

34. Hancox, N. L., and Brunton, J. H., Phil. Trans. Roy. Soc. (London), Vol. A. 260, p. 121, 1966.

35. Thiruvengadam, A., Rudy, S. L., and Gunasekaran, M., "Experimental and Analytical Investigations on Liquid Impact Erosion," ASTM STP 474, pp. 249-287, 1970.

36. Benjamin, T. B., and Ellis, A. T., "The Collapse of Cavitation Bubbles and the Pressures Thereby Produced Against Solid Boundaries," Phil. Trans., Roy. Soc. (London), Vol. 260A, pp. 221-240, 1966.

37. Tulin, M. P., "On the Creation of Ultra-Jets," L. I. Sedov 60th Anniversary Volume, Problems of Hydrodynamics and Continuum Mechanics, Moscow, 1969.

38. Mitchell, T. M., and Hammitt, F. G., "Collapse of a Spherical Bubble in a Pressure Gradient," ASME Cavitation Forum, May 1970.

39. Plesset, M. S. and Chapman, R. B., "Collapse of an Initially Spherical Vapor Cavity in the Neighborhood of a Solid Boundary," Rep. 85-49, Cal. Inst. of Tech., Div. of Engrg. and Appl. Science, June 1970.

40. Bowden, F. P., and Brunton, J. H., "The Deformation of Solids by Liquid Impact at Supersonic Speeds," Proc. Roy. Soc., Vol. A263, pp. 433-450, 1961.

41. McClintock, F. A., and Argon, A. S., (Eds.), Mechanical Behavior of Materials, Addison-Wesley Publishing Co., Inc., Reading, Mass., 1966.

42. Goldsmith, W., "Impact," The Theory and Physical Behavior of Colliding Solids," Edward Arnold (Publishers), Ltd., 1960.

43. Tabor, D., "The Hardness of Metals," Oxford, The Clarendon Press, 1951.

44. Thiruvengadam, A., "Prediction of Cavitation Damage," Ph.D. Thesis, Indian Institute of Science, Bangalore-12, India, 1961.

45. Thiruvengadam, A., "A Unified Theory of Cavitation Damage," Trans. ASME, Jour. Basic Eng., Vol. 85, Series D, September 1963, pp. 365-376.

46. Hickling, R., "Some Physical Effects of Cavity Collapse in Liquids," Trans. ASME, Jour. Basic Engrg., Series D., Vol. 88, No. 1, pp. 229-235, 1966.

47. Plesset, M. A., "Bubble Dynamics", in Cavitation in Real Fluids (Robert Davis, ed.), pp. 1-18, Elsevier Publishing Company, Amsterdam, 1964.

48. Ivany, R. D., Hammitt, F. G., and Mitchell, R. M., "Cavitation Bubble Collapse Observations in a Venturi," Trans. ASME, J. Basic Engrg., Vol. 88, No. 3, Series D, 1966, pp. 649-657.

49. Johnson, V. E., Jr., "Cavitation Inception and Damage," Schiffstechnik, Bd. 13, pp. 19-26, Heft 65, 1966.

50. A Guide for Fatigue Testing and the Statistical Analysis of Fatigue Data (supplement to Manual on Fatigue Testing, STP No. 91) ASTM Special Technical Publication No. 91-A, Second Edition, 1963.

51. Wood, G. M., Knudsen, L. K., and Hammitt, F. G., "Cavitation Damage Studies with Rotating Disk," Trans. ASME, J. Basic Engrg. Vol. 89, No. 1, Series D., 1967, pp. 98-110.

52. Holl, J. W., "Limited Cavitation," Cavitation State of Knowledge, ASME, pp. 26-64, 1969.

Table 1 - Summary of Scaling Parameters

	Jet Impact		Spherical Collapse
	Stagnation Pressure (Macro-jet)	Water Hammer Pressure (Micro-jet)	
	$\Theta = \frac{\sigma}{\delta}(\Delta\sigma)^{\frac{1}{2}}\exp\left[\frac{-2.67}{W(\Delta\sigma)}\right]$	$\Theta = \frac{\sigma}{\delta M}(\Delta\sigma)^{\frac{1}{2}}\exp\left[\frac{-2.67}{W(\Delta\sigma)}\right]$	$\Theta = \frac{\sigma}{\delta}(\Delta\sigma)^{\frac{1}{2}}\cdot \exp\left[\frac{2}{3}\alpha - \frac{2.67}{W(\Delta\sigma)}\right]$
Erosion number	$\Theta = \frac{I_e}{\frac{1}{2}\rho V_o^3}$	Same	Same
Relative nuclei size	$\delta = \bar{d}/\ell$	Same	Same
Weber Number	$W = \frac{\frac{1}{2}\rho V_o^2 \bar{d}}{\gamma}$	Same	Same
Cavitation number	$\sigma = \frac{p_o - p_v}{\frac{1}{2}\rho V_o^2}$	Same	Same
Cavitation inception number	$\sigma_i = \frac{p_i - p_v}{\frac{1}{2}\rho V_o^2}$	Same	Same
Degree of cavitation	$\Delta\sigma = \sigma_i - \sigma$	Same	Same
Mach number	None	$M = V_o/C$	
Damping number	None	None	$\alpha = P_o/Q_o$

TABLE 2

Range of Nuclei Size, Velocity and Weber Number
for Laboratory Experiments and for Prototype Operations

$\rho = 1.98$ slugs/ft^3

$\gamma = .005$ lb/ft

Mean Nuclei Size $\bar{d}$, ft	Velocity V_o, fps	Weber Number $W = \frac{\frac{1}{2}\rho V_o^2 d}{\gamma}$
10^{-5}	50	5
	100*	20*
	200*	80*
10^{-4}	50	50
	100	200
	200	800
10^{-3}	50	500
	100**	2000**
	200**	8000**
10^{-2}	50	5000
	100	20000
	200	80000

*Range of values likely for experiments in the laboratory.

**Range of values likely for prototype operation.

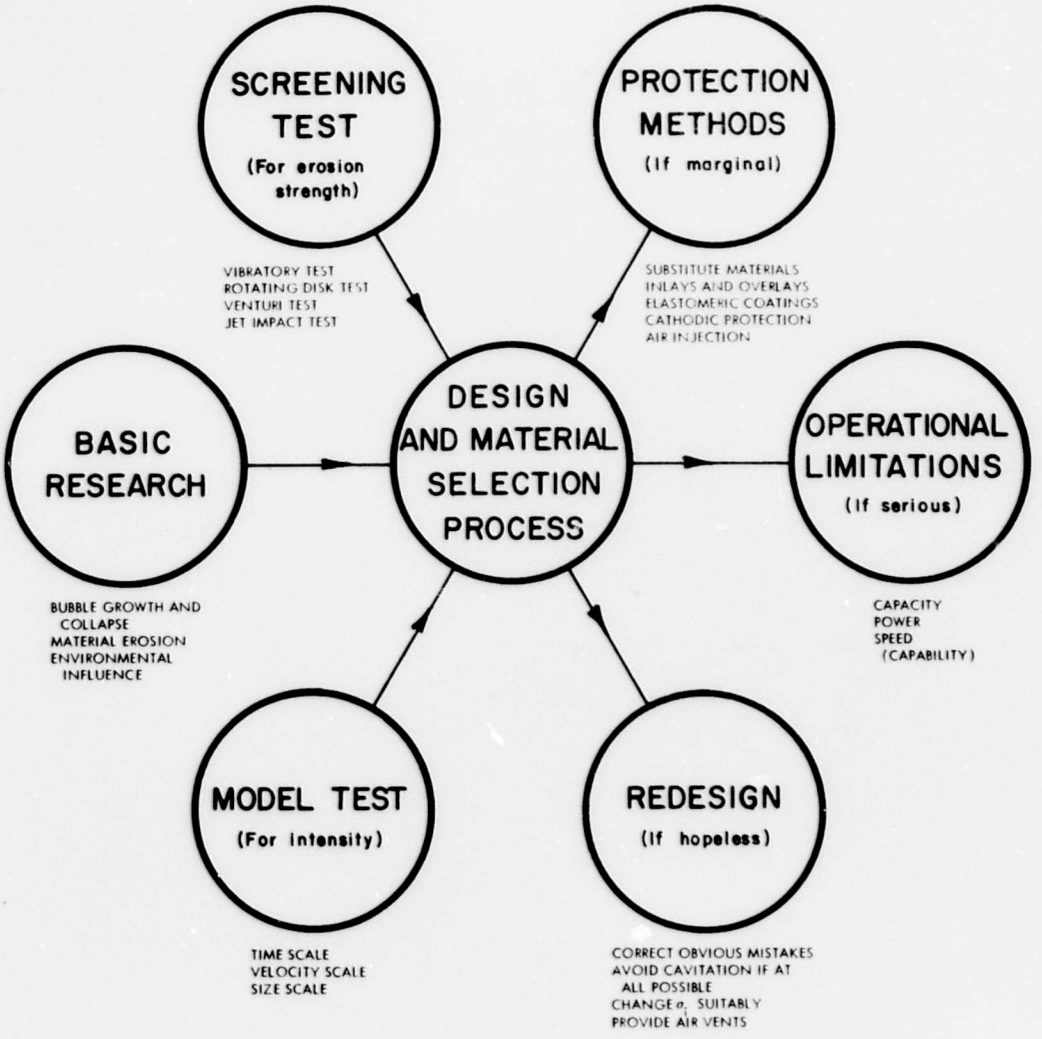

FIGURE 1 - ENGINEERING ASPECTS OF CAVITATION EROSION

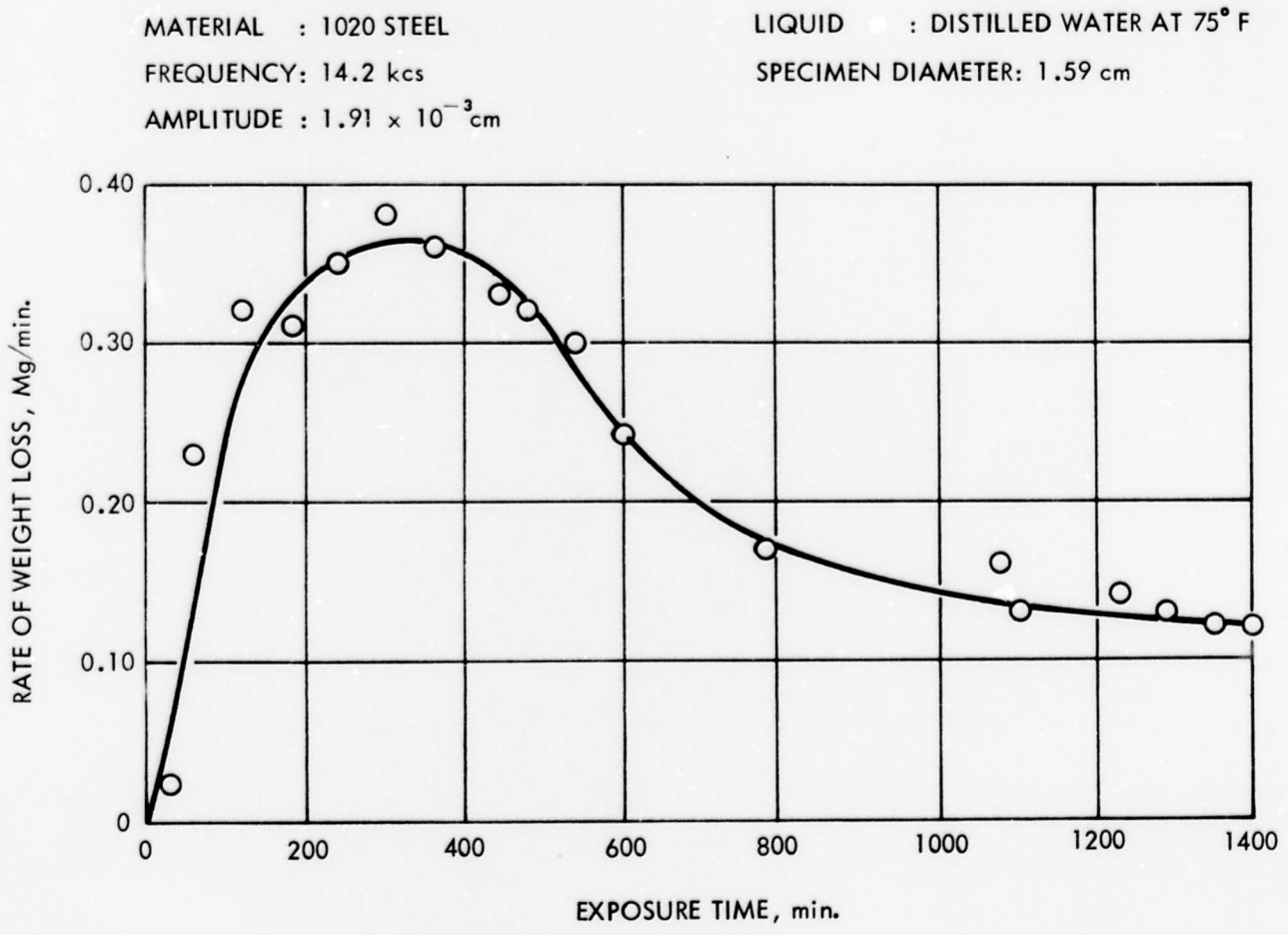

FIGURE 2 - RELATION BETWEEN EXPOSURE TIME AND CAVITATION EROSION RATE OF SAE 1020 STEEL

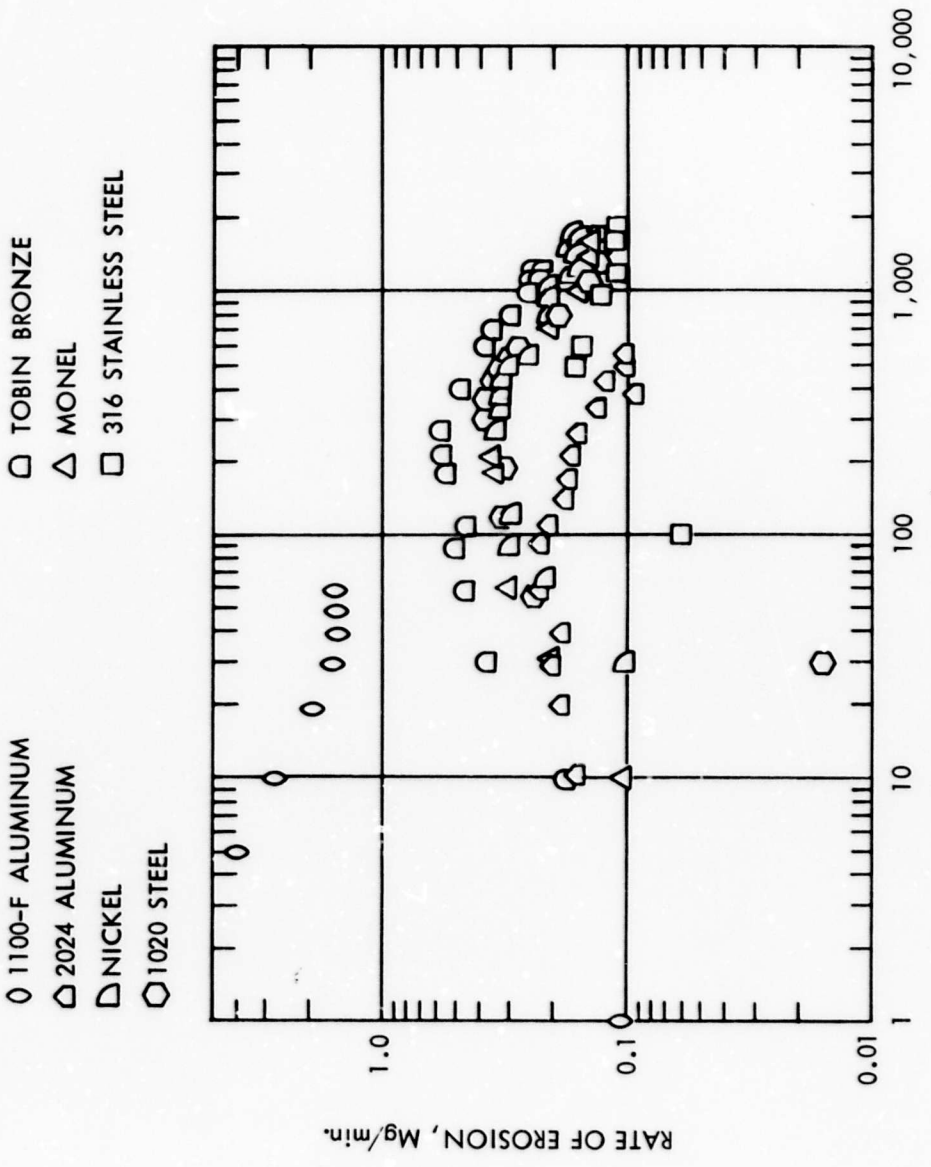

FIGURE 3 - EROSION RATE AND EXPOSURE TIME RELATIONS FOR SEVEN MATERIALS

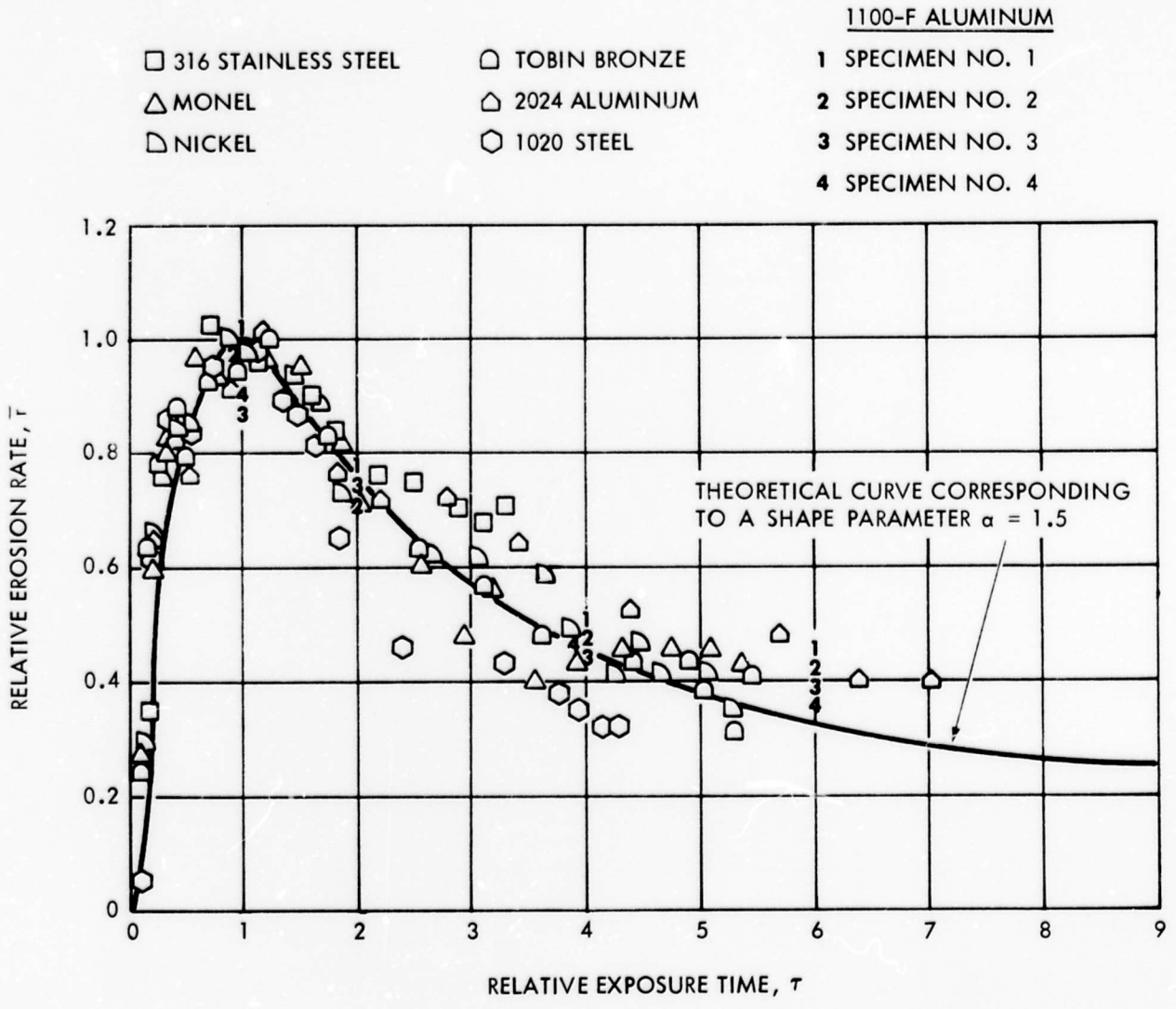

FIGURE 4 - RELATIVE EROSION RATE AS A FUNCTION OF RELATIVE EXPOSURE TIME FOR THE SEVEN MATERIALS

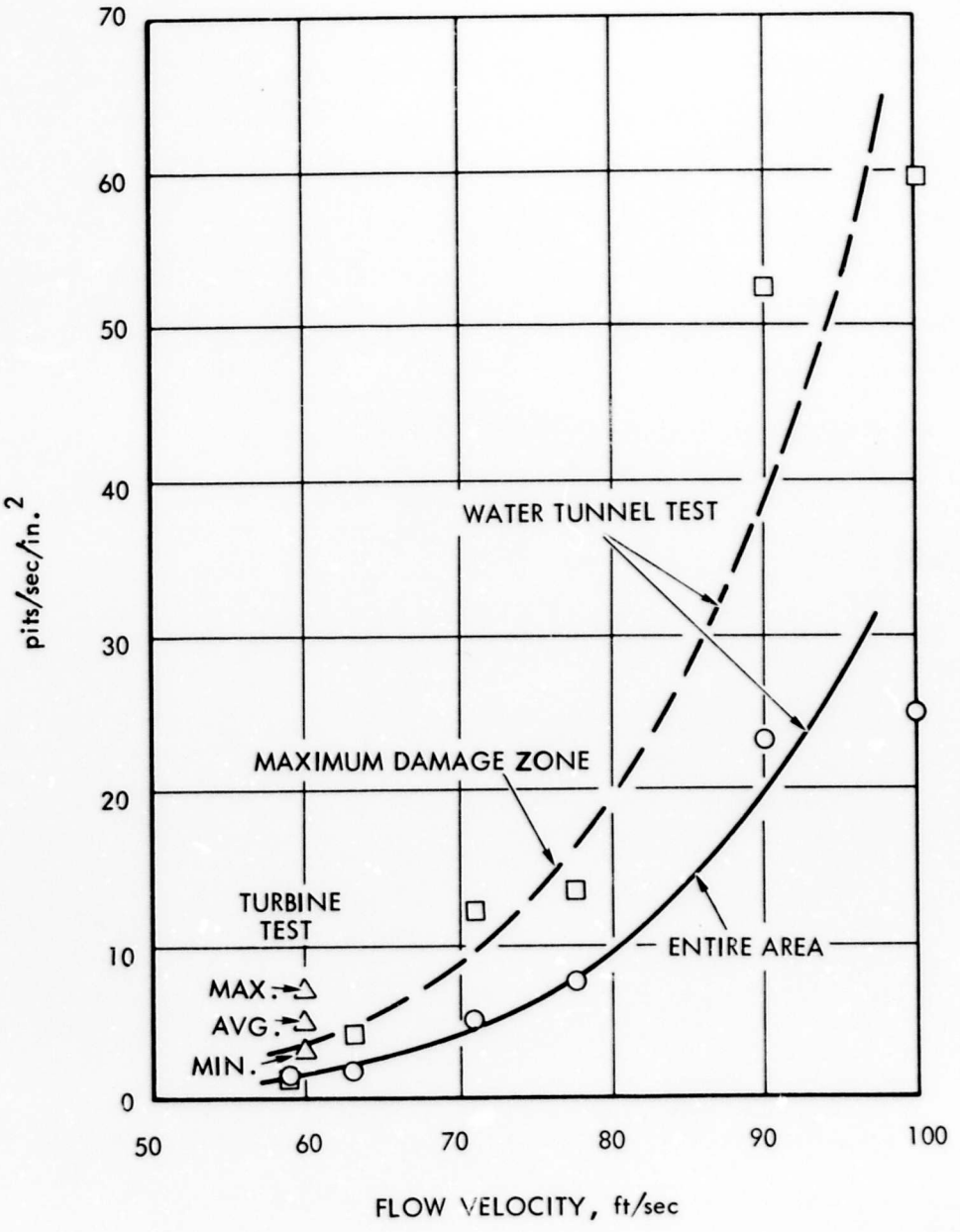

FIGURE 5 - COMPARISON OF TURBINE PITTING RATE WITH WATER TUNNEL TEST RESULTS (KNAPP, 1956)

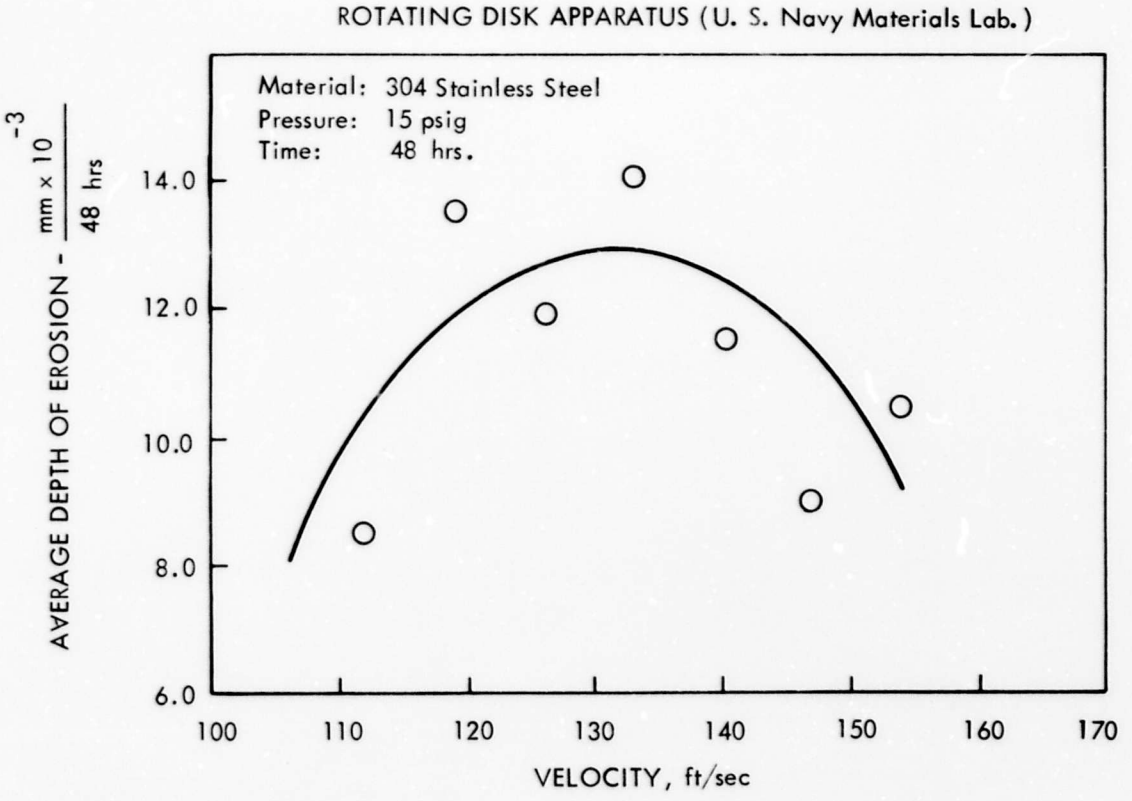

FIGURE 6 - EFFECT OF VELOCITY ON RATE OF DEPTH OF EROSION

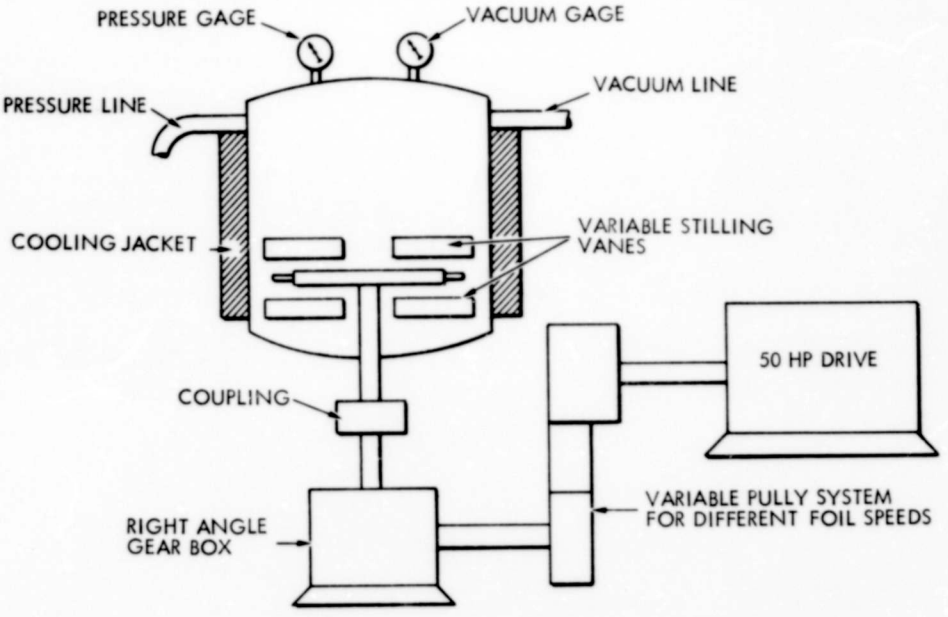

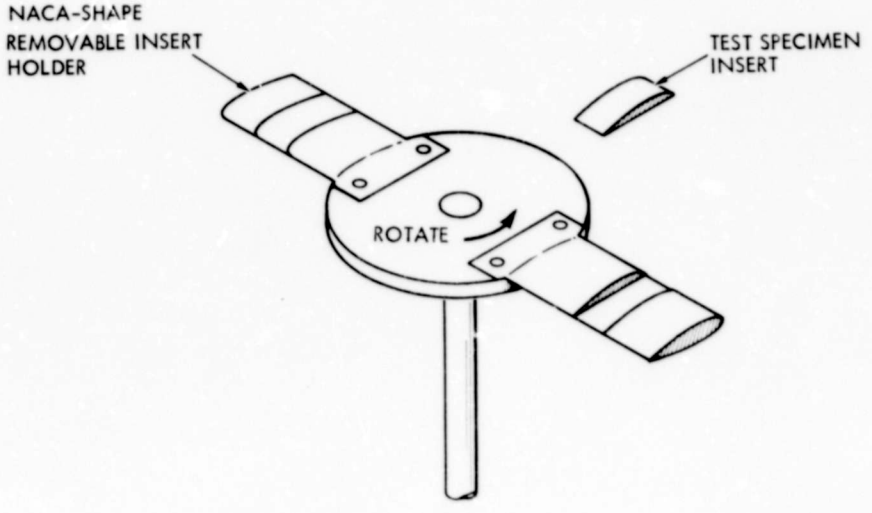

FIGURE 7A - ROTATING FOIL FACILITY SCHEMATIC

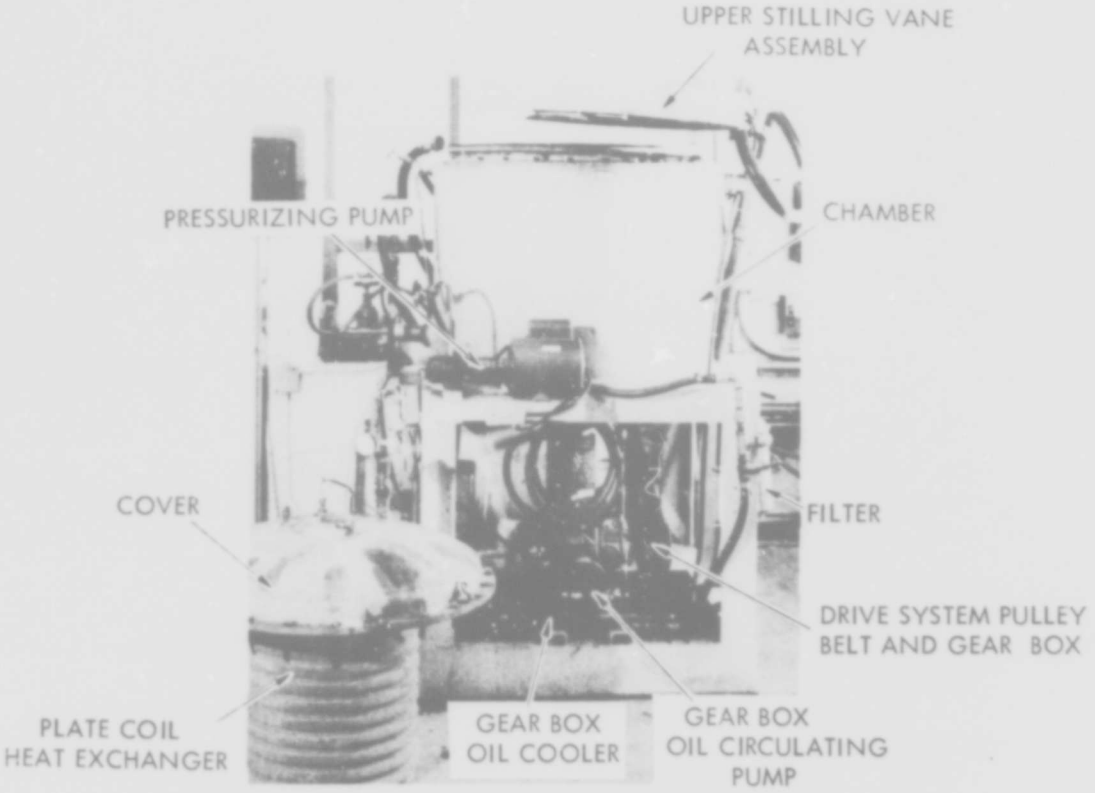

NOTE: DRIVE MOTOR IS POSITIONED BEHIND FACILITY

FIGURE 7B - ROTATING FOIL APPARATUS

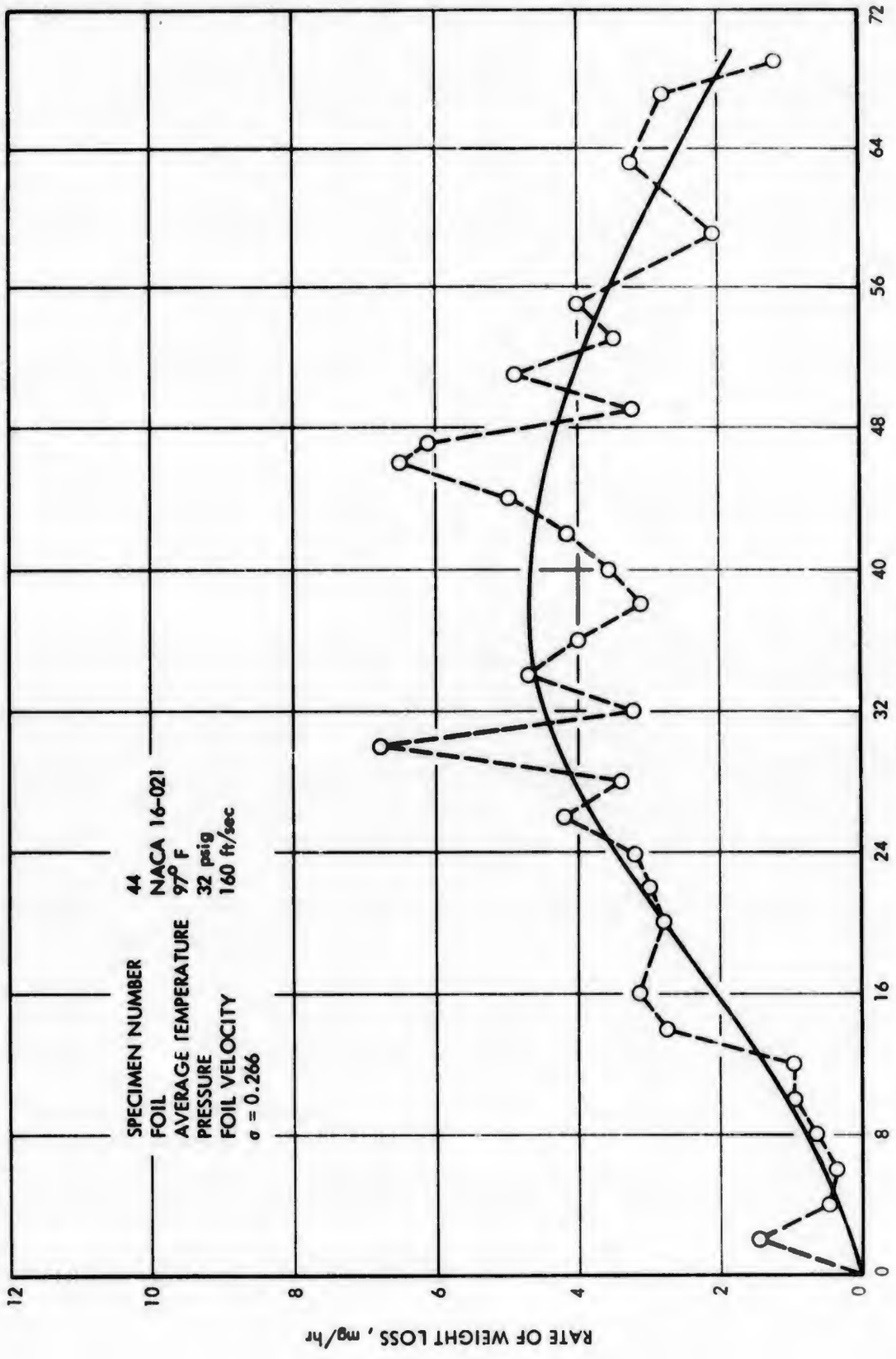

FIGURE 8 - RATE OF WEIGHT LOSS VS. TESTING TIME FOR THE FULL SIZE (3" CHORD LENGTH) HYDROFOIL.

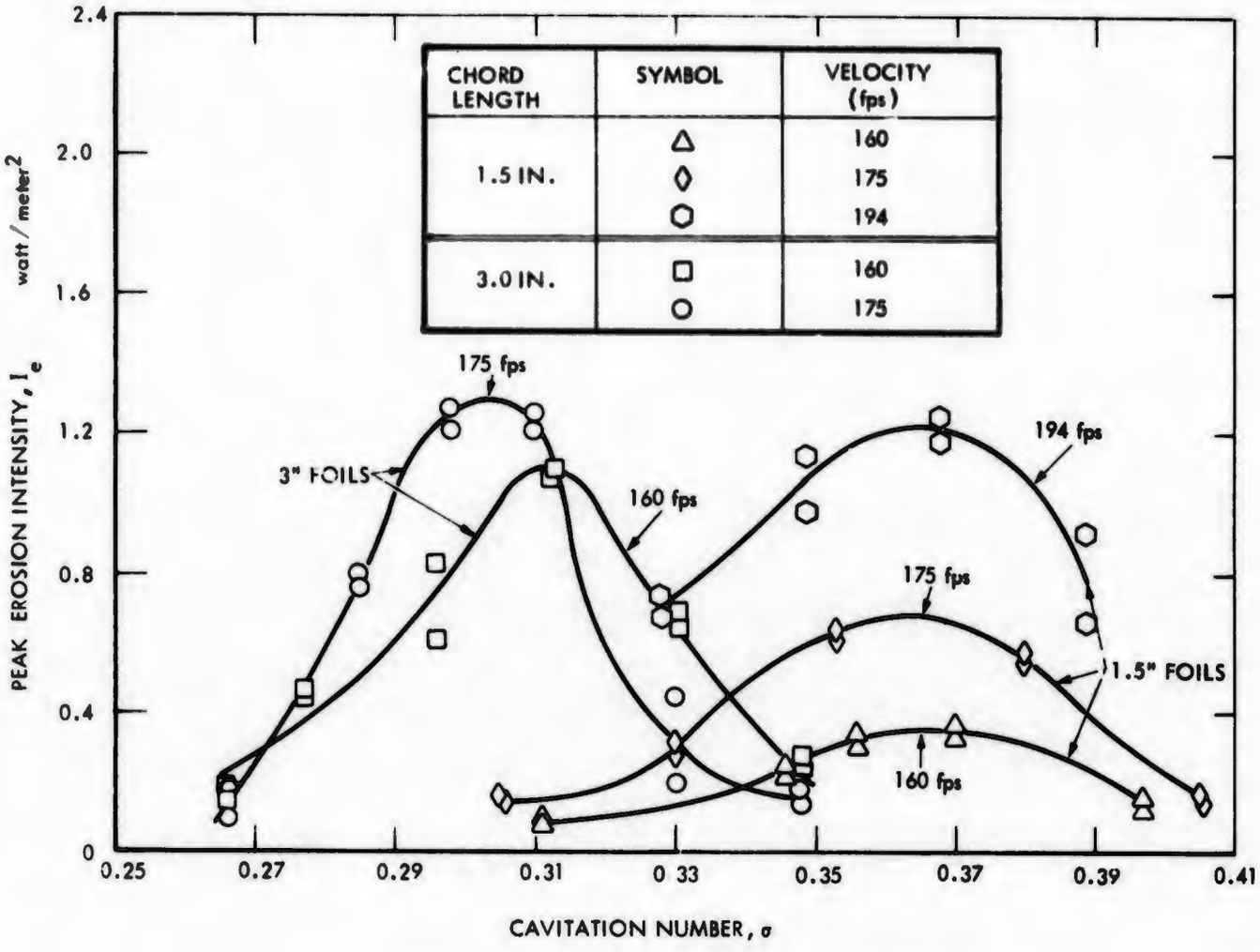

FIGURE 9 - RELATIONSHIP BETWEEN PEAK INTENSITY OF EROSION AND CAVITATION NUMBER FOR NACA-16-021 FOILS

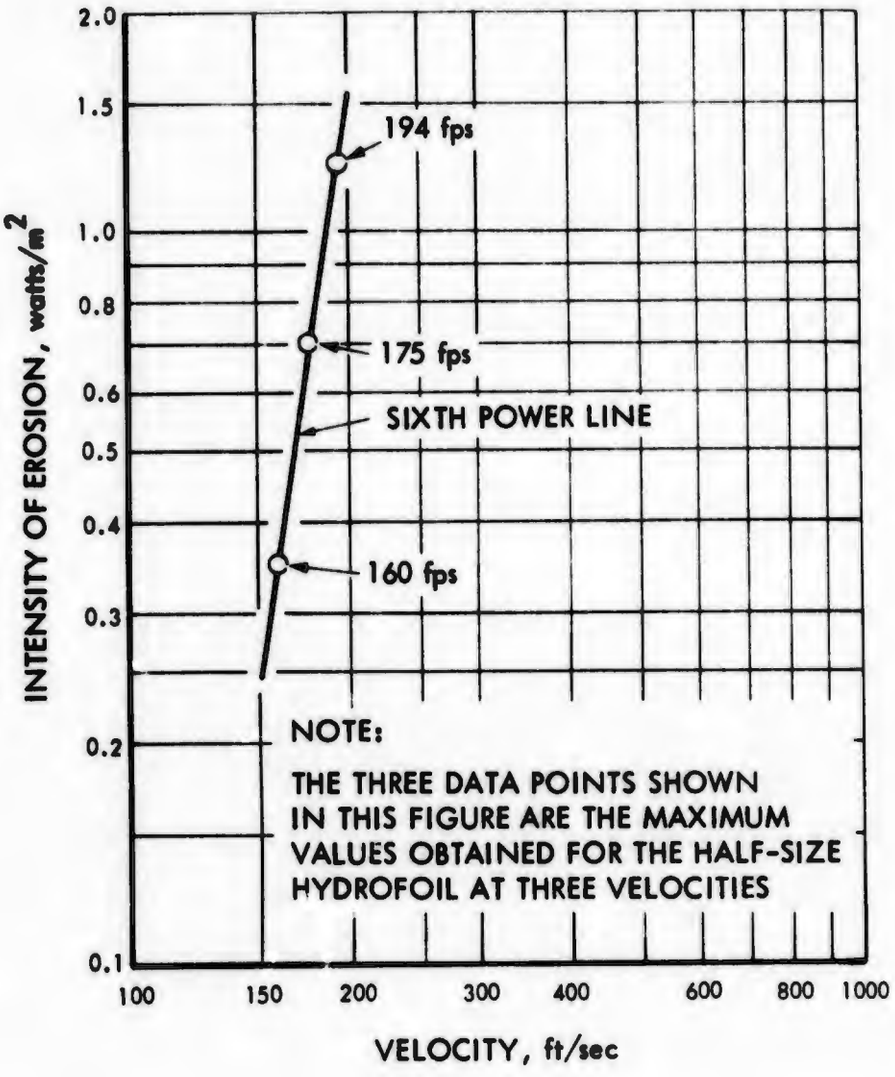

FIGURE 10 - DATA FOR 1½ in. NACA-16-021 HYDROFOIL AT THREE VELOCITIES COMPARED WITH SIXTH POWER LAW

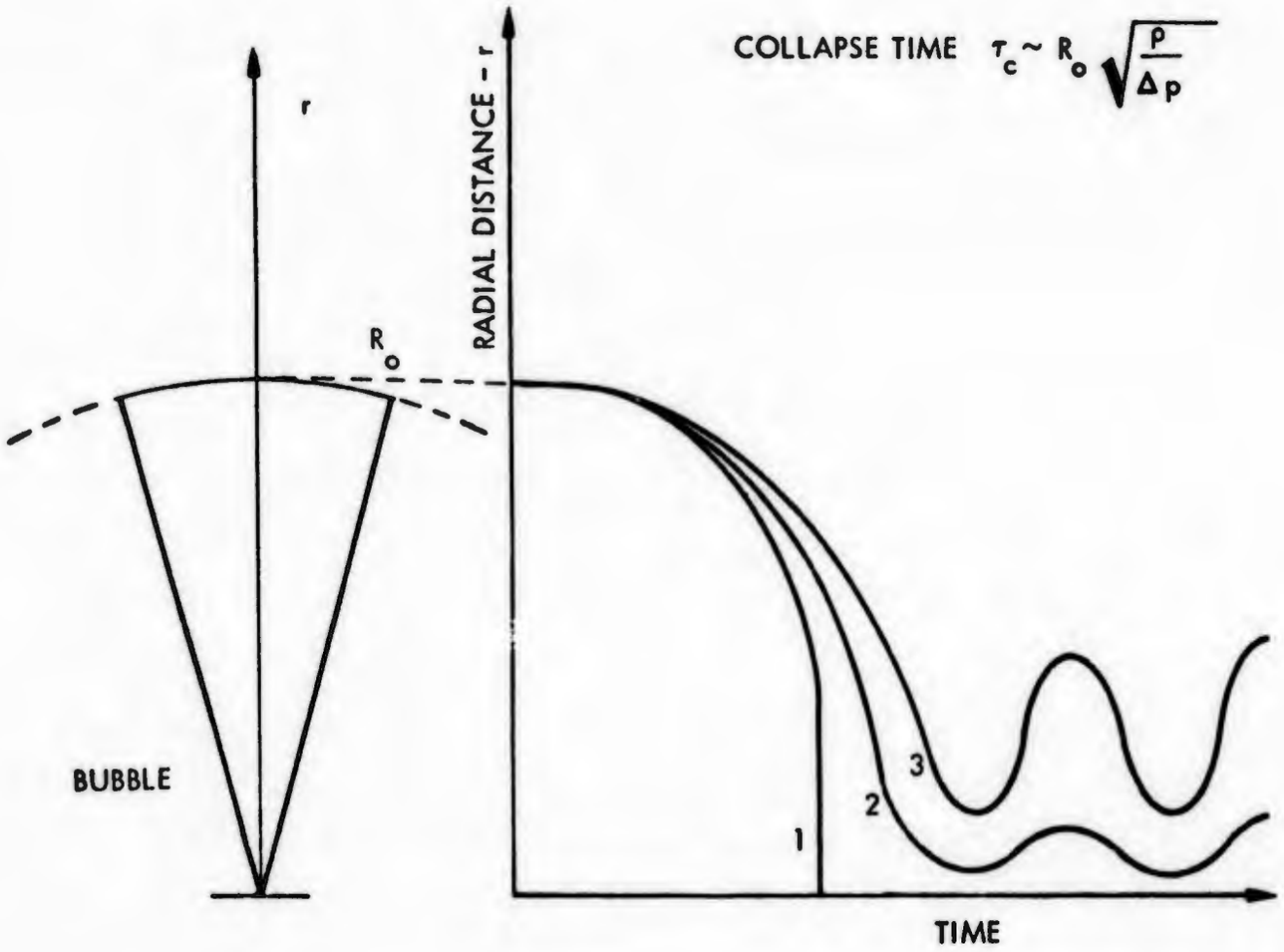

1. EMPTY BUBBLE IN AN INCOMPRESSIBLE LIQUID
2. WITH COMPRESSIBLE GAS INSIDE THE BUBBLE
3. INCLUDING COMPRESSIBILITY OF THE LIQUID; SURFACE TENSION TENDS TO INCREASE THE COLLAPSE RATE, VISCOSITY TENDS TO DECREASE THE COLLAPSE RATE

FIGURE 11 - SPHERICAL COLLAPSE (Rayleigh, 1917, et al)

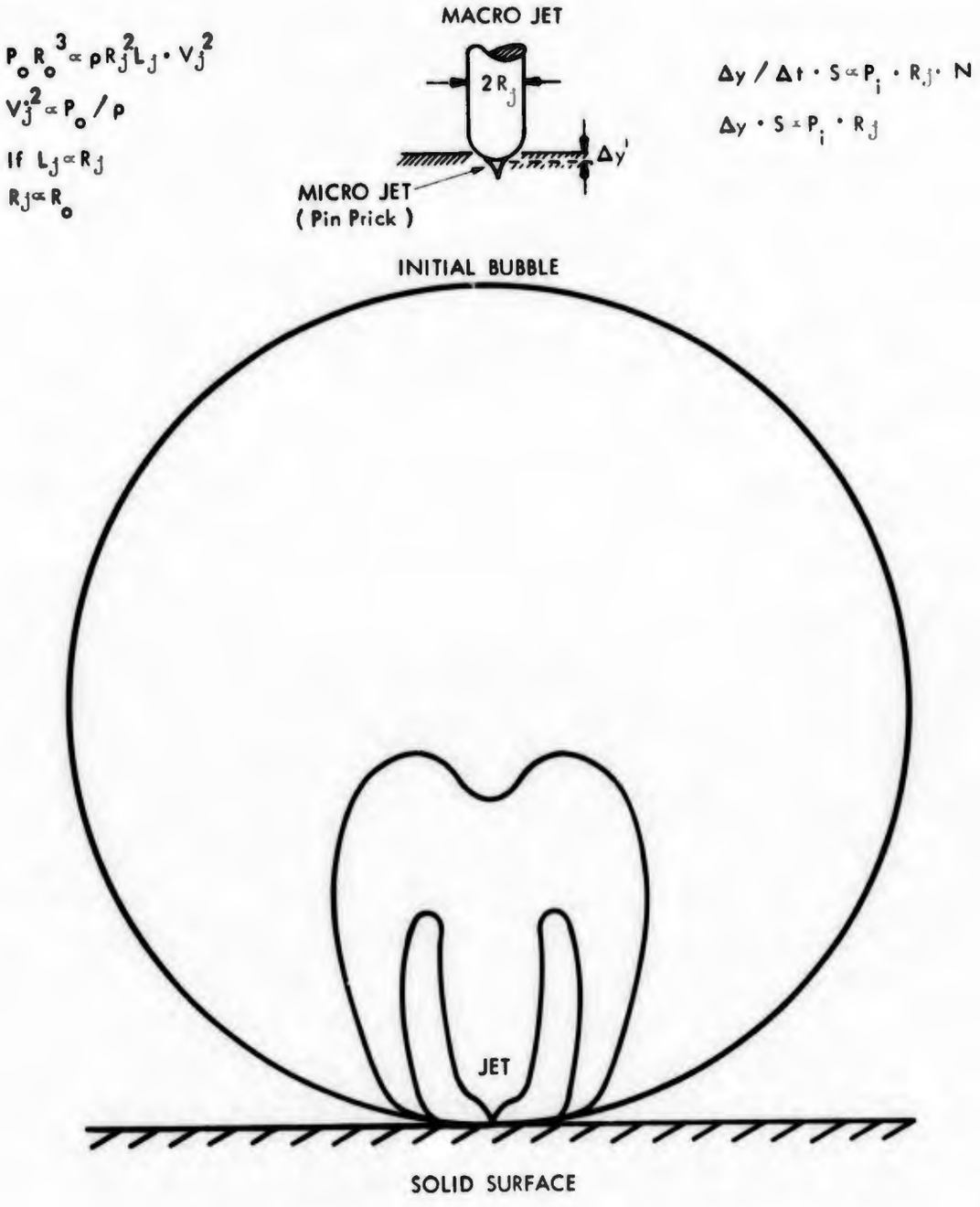

FIGURE 12 - COLLAPSE IN THE NEIGHBORHOOD OF A SOLID BOUNDARY (PLESSET AND CHAPMAN, 1970)

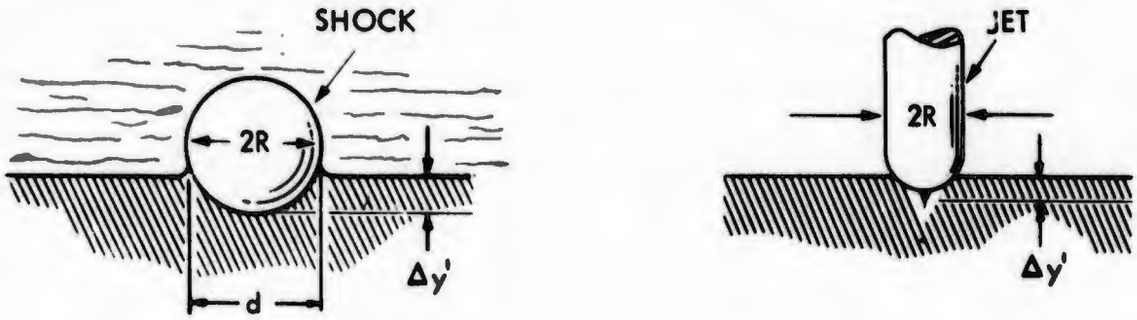

Single Impact	$\Delta y' \cdot S_e \propto P_i \cdot R$
Multiple Impact	$\frac{\Delta y}{\Delta t} \cdot S_e \propto P_i \cdot R \cdot f$

SPHERICAL COLLAPSE	STAGNATION PRESSURE (Macrojet)	WATER-HAMMER PRESSURE (Microjet)
$P_i \propto P_o (R_o / R_c)^2$	$P_i \propto \frac{1}{2} \rho V_j^2$	$P_i \propto \rho C V_j$
For example:	$P_i \propto \frac{1}{2} \rho \cdot P_o / \rho$	$P_i \propto \rho C (P_o / \rho)^{\frac{1}{2}}$
$R_o / R_c \propto \exp (P_o / Q_o)$	$P_i \propto P_o$	$P_i \propto C (\rho P_o)^{\frac{1}{2}}$

FIGURE 13 - PARAMETERS GOVERNING INDENTATION AND RATE OF EROSION

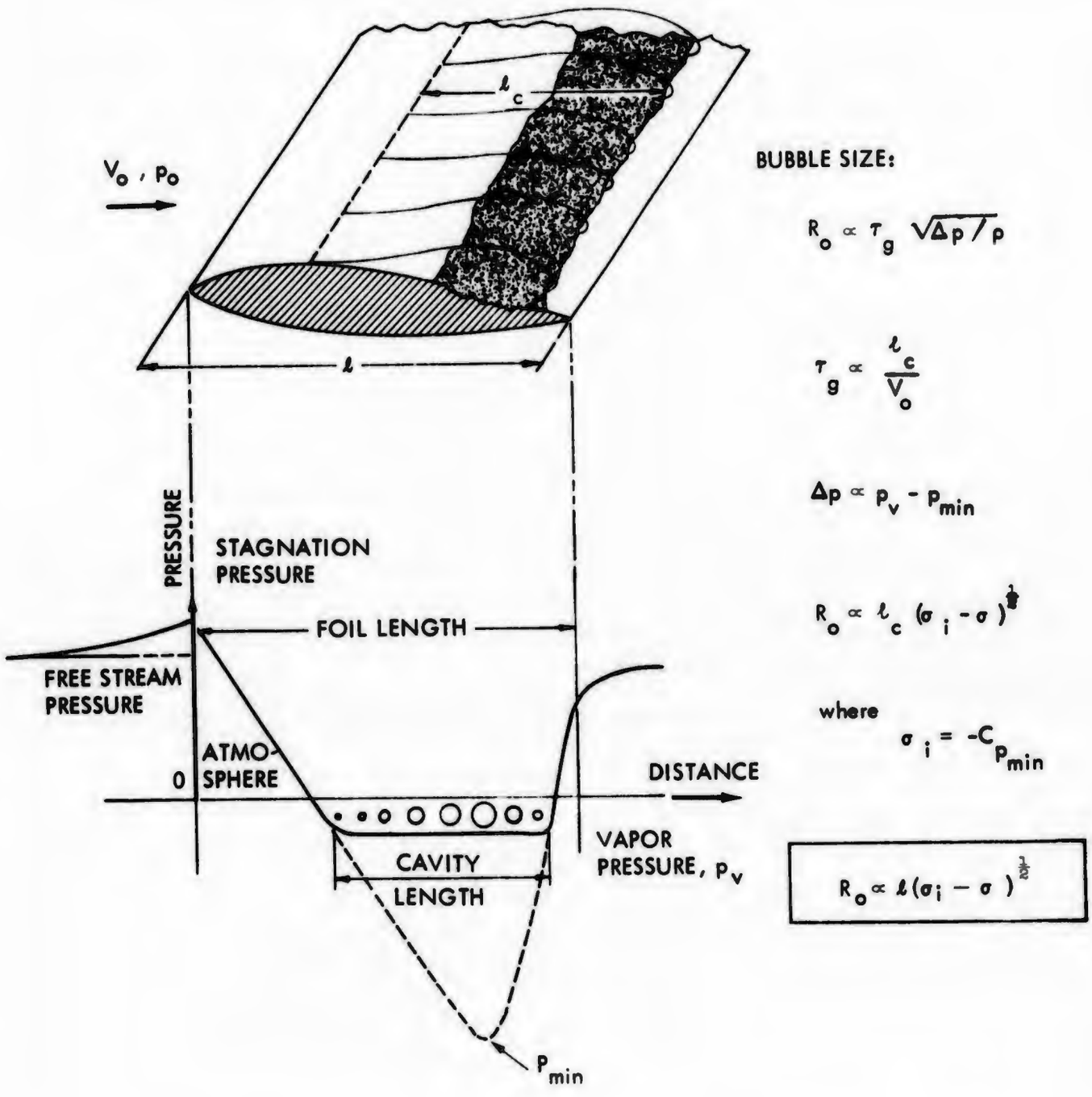

FIGURE 14 - PARAMETERS GOVERNING THE MAXIMUM SIZE OF THE BUBBLES

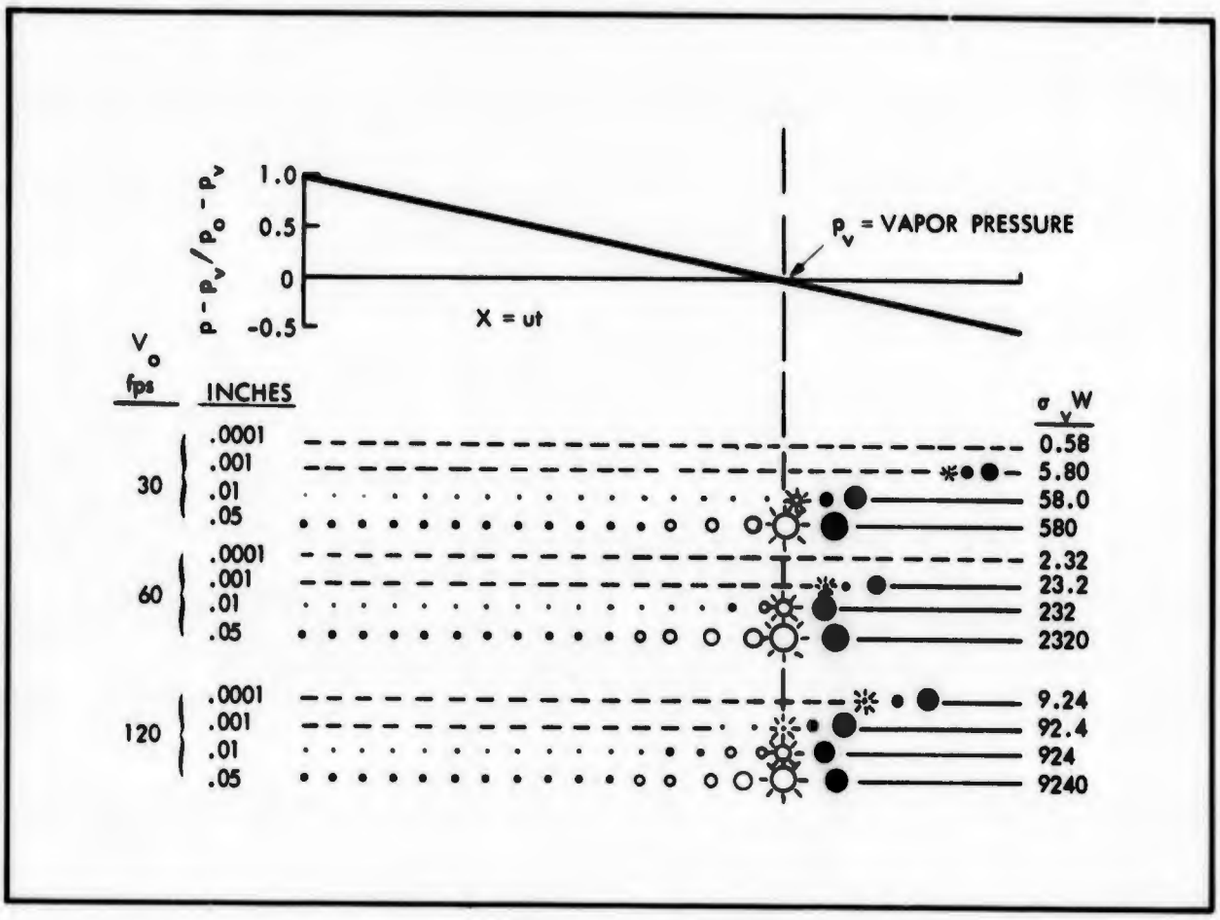

FIGURE 15 - SPHERICAL GAS BUBBLE GROWTH, $\sigma_v = 0.2$

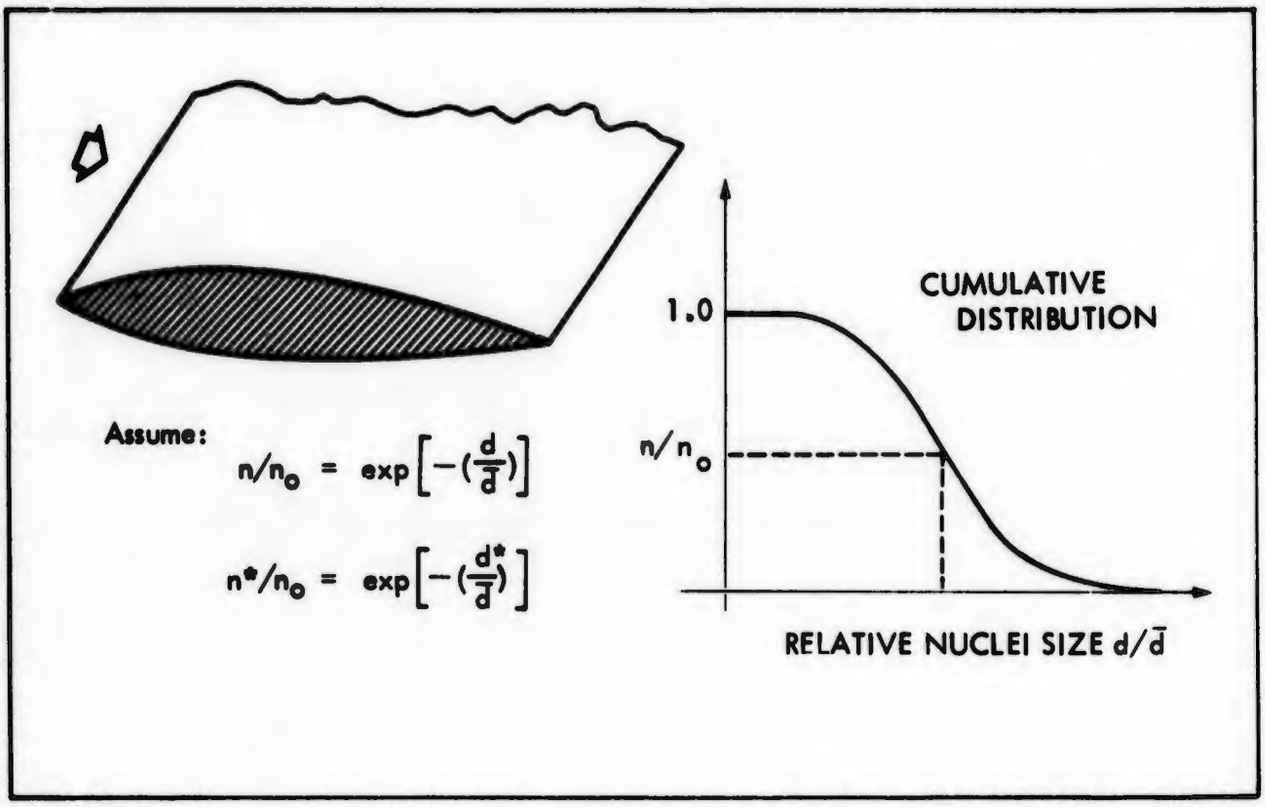

FIGURE 16 - STATISTICAL DISTRIBUTION OF NUCLEI SIZES

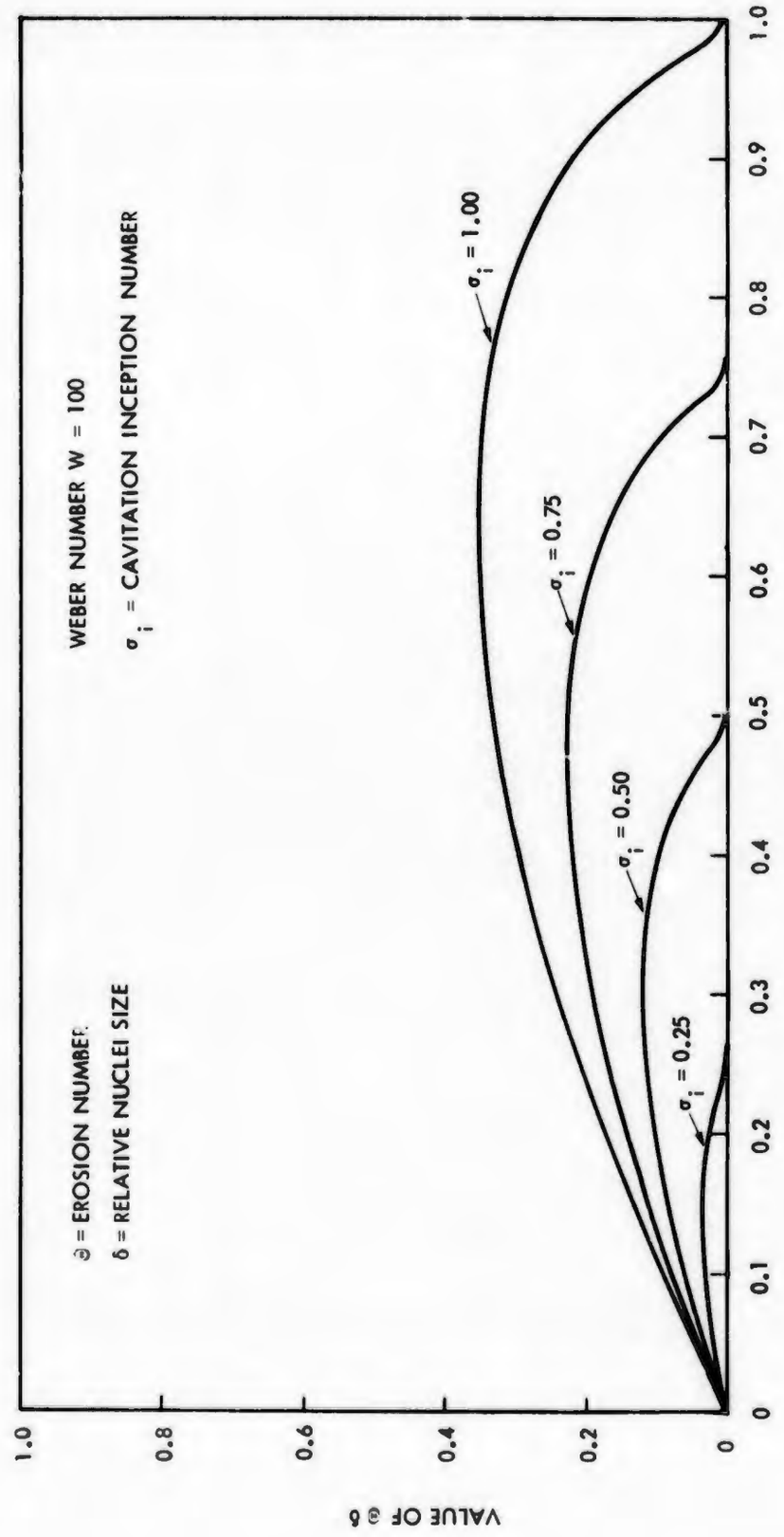

FIGURE 17 - EFFECT OF CAVITATION NUMBER ON THE EROSION NUMBER

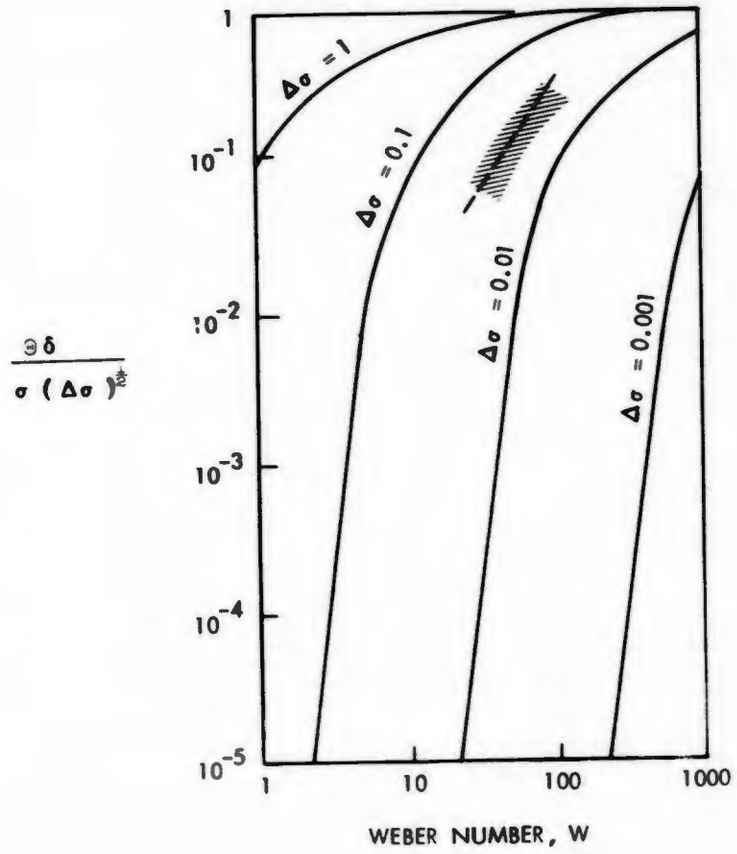

$$\Im = \frac{\frac{\Delta\gamma}{\Delta t} \cdot \xi}{\frac{1}{2}\rho V_o^3}$$

$$\sigma = p_o - p_v / \frac{1}{2}\rho V_o^2$$

$$\Delta\sigma = (\sigma_i - \sigma)$$

$$\delta = \bar{d}/\ell$$

$$W = \frac{1}{2}\rho V_o^2 \bar{d} / \gamma$$

If $\Im \propto (W)^{1.5}$

Then $W \propto V_o^2$

$\eta \propto V_o^3$

$I_e \propto \Im V_o^3$

$I_e \propto V_o^6$

$$\frac{\Im \delta}{\sigma (\Delta\sigma)^{\frac{1}{2}}} = \exp\left[\frac{-2.67}{W(\Delta\sigma)}\right]$$

① SIXTH POWER LAW
② EFFECT OF SIZE
③ EFFECT OF CAVITATION PARAMETER
④ SUGGESTIONS FOR MODELING: $\Delta\Im \sim 0.1$, $W > 500$, δ Constant

FIGURE 18 - EFFECT OF WEBER NUMBER ON CAVITATION EROSION

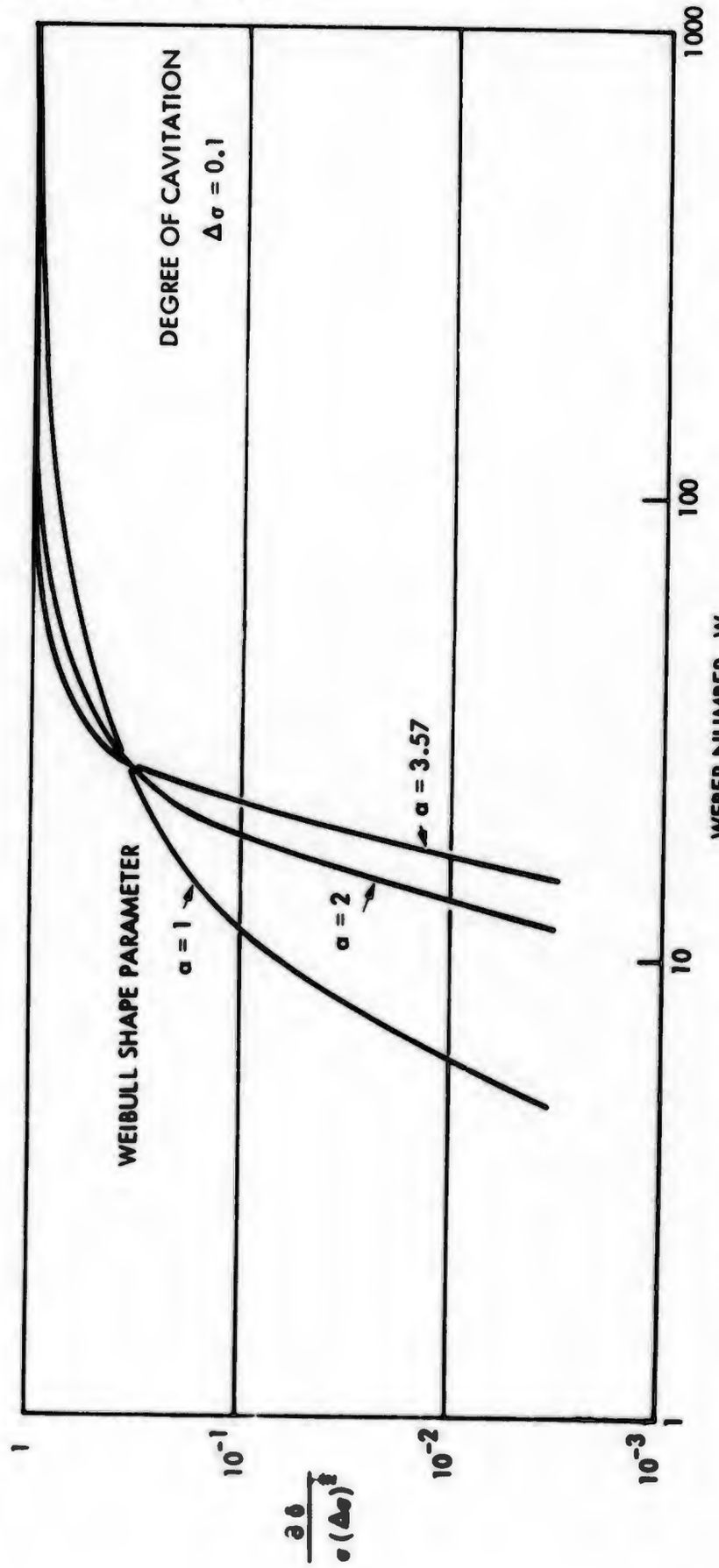

FIGURE 19 - INFLUENCE OF DIFFERENT NUCLEI DISTRIBUTIONS ON CAVITATION EROSION